Review

Satellite remote sensing of active fires: History and current status, applications and future requirements

Martin J. Wooster [a,p,*], Gareth J. Roberts [b], Louis Giglio [c], David P. Roy [d], Patrick H Freeborn [e], Luigi Boschetti [f], Chris Justice [g], Charles Ichoku [h], Wilfrid Schroeder [i], Diane Davies [j,k], Alistair M.S. Smith [f], Alberto Setzer [l], Ivan Csiszar [m], Tercia Strydom [n], Philip Frost [o], Tianran Zhang [p], Weidong Xu [p], Mark C de Jong [p], Joshua M. Johnston [q], Luke Ellison [r], Krishna Vadrevu [s], Aaron M. Sparks [f], Hannah Nguyen [a,p], Jessica McCarty [t], Veerachai Tanpipat [u], Chris Schmidt [v], Jesus San-Miguel-Ayanz [w]

[a] Leverhulme Center for Wildfire, Environment & Society, c/o Dept. of Geography, Kings College London, Aldwych, London WC2B 4BG, UK
[b] Geography and Environmental Science, University of Southampton, Southampton, UK
[c] Department of Geographical Sciences, University of Maryland, College Park, MD, USA
[d] Department of Geography, Environment, and Spatial Sciences, and Center for Global Change and Earth Observations, Michigan State University, East Lansing, MI, USA
[e] Missoula Fire Sciences Laboratory, Rocky Mountain Research Station, USDA Forest Service, Missoula, MT, USA
[f] Department of Forest, Rangeland, and Fire Sciences, University of Idaho, Moscow, ID, USA
[g] Department of Geographical Sciences, University of Maryland, College Park, MD, USA
[h] Interdisciplinary Studies, Atmospheric and Environmental Sciences, Howard University, Washington, District of Columbia, USA
[i] NOAA/NESDIS/OSPO Satellite Analysis Branch, College Park, MD, USA
[j] Trigg-Davies Consulting Ltd., Malvern, UK
[k] GSFC, Science Systems and Applications Inc., Lanham, Maryland, United States
[l] Centro de Previsão de Tempo e Estudos Climáticos/Instituto Nacional de Pesquisas Espaciais, Programa de Monitoramento de Queimada por Satélites, 12227-010, São José dos Campos, SP, Brazil
[m] NOAA/NESDIS Center for Satellite Applications and Research (STAR), College Park, MD, USA
[n] Scientific Services, South African National Parks, Skukuza, South Africa
[o] iMMAP Middle East, Mecca St. 145, Amman, Jordan
[p] NERC National Centre for Earth Observation (NCEO), c/o Dept. of Geography, Kings College London, Aldwych, London WC2B 4BG, UK
[q] Canadian Forest Service, Great Lakes Forestry Centre, Sault Ste. Marie, ON, Canada
[r] Science Systems and Applications, Inc. (SSAI), NASA Goddard Space Flight Center, Greenbelt, MD 20771, USA
[s] NASA Marshall Space Flight Center, Huntsville, Alabama 35811, USA
[t] Department of Geography and Geospatial Analysis Center, Miami University, Oxford, OH, USA
[u] Upper ASEAN Wildland Fire Special Research Unit, Kasetsart University, Bkk, Thailand
[v] Cooperative Institute for Meteorological Satellite Studies, Space Science Engineering Center, University of Wisconsin-, Madison, USA
[w] European Commission Joint Research Centre, Ispra, Italy

ARTICLE INFO	ABSTRACT
Editor: Marie Weiss *Keywords:* Active fire	Landscape fire is a widespread, somewhat unpredictable phenomena that plays an important part in Earth's biogeochemical cycling. In many biomes worldwide fire also provides multiple ecological benefits, but in certain circumstances can also pose a risk to life and infrastructure, lead to net increases in atmospheric greenhouse gas concentrations, and to degradation in air quality and consequently human health. Accurate, timely and

* Corresponding author at: Leverhulme Center for Wildfire, Environment & Society, c/o Dept. of Geography, Kings College London, Aldwych, London WC2B 4BG, UK

E-mail addresses: martin.wooster@kcl.ac.uk (M.J. Wooster), G.J.Roberts@soton.ac.uk (G.J. Roberts), lgiglio@umd.edu (L. Giglio), roydavi1@msu.edu (D.P. Roy), patrick.h.freeborn@usda.gov (P.H. Freeborn), luigi@uidaho.edu (L. Boschetti), cjustice@umd.edu (C. Justice), charles.ichoku@howard.edu (C. Ichoku), wilfrid.schroeder@noaa.gov (W. Schroeder), diane.k.davies@nasa.gov (D. Davies), alistair@uidaho.edu (A.M.S. Smith), alberto.setzer@inpe.br (A. Setzer), ivan.csiszar@noaa.gov (I. Csiszar), tercia.strydom@sanparks.org (T. Strydom), pfrost@immap.org (P. Frost), tianran.zhang@kcl.ac.uk (T. Zhang), weidong.xu@kcl.ac.uk (W. Xu), mark.dejong@kcl.ac.uk (M.C. de Jong), Joshua.Johnston@canada.ca (J.M. Johnston), krishna.p.vadrevu@nasa.gov (K. Vadrevu), asparks@uidaho.edu (A.M. Sparks), hannah.nguyen@kcl.ac.uk (H. Nguyen), mccartjl@miamioh.edu (J. McCarty), fforvrc@ku.ac.th (V. Tanpipat), chris.schmidt@ssec.wisc.edu (C. Schmidt), jesus.san-miguel@ec.europa.eu (J. San-Miguel-Ayanz).

frequently updated information on landscape fire activity is essential to improve our understanding of the drivers and impacts of this form of biomass burning, as well as to aid fire management. This information can only be provided using satellite Earth Observation (EO) approaches, and remote sensing of active fire is one of the key techniques used. This form of EO is based on detecting the signature of the (mostly infrared) electromagnetic radiation emitted as biomass burns. Since the early 1980's, active fire (AF) remote sensing conducted using low Earth orbit (LEO) satellites has been deployed in certain regions of the world to map the location and timing of landscape fire occurrence, and from the early 2000's global-scale information updated multiple times per day has been easily available to all. Geostationary (GEO) satellites provide even higher frequency AF information, more than 100 times per day in some cases, and both LEO- and GEO-derived AF products now often include estimates of a fires characteristics, such as its fire radiative power (FRP) output, in addition to the fires detection. AF data provide information relevant to fire activity ongoing when the EO data were collected, and this can be delivered with very low latency times to support applications such as air quality forecasting. Here we summarize the history of achievements in the field of active fire remote sensing, review the physical basis of the approaches used, the nature of the AF detection and characterization techniques deployed, and highlight some of the key current capabilities and applications. Finally, we list some important developments we believe deserve focus in future years.

1. Introduction

Landscape fire is a widespread natural disturbance agent involved in Earth's biogeochemical cycling, but one that can be greatly influenced by human actions, including in relation to climate and environmental change. Fire provides multiple ecological benefits (McLauchlan et al., 2020) – but in certain circumstances also poses a risk to life and infrastructure (Duff and Penman, 2021). In areas of substantial landscape fire activity and in regions downwind, air quality can also be seriously degraded - leading to major human health impacts and hundreds of thousands of early deaths per year worldwide (Roberts and Wooster, 2021). Deforestation fires, other fire involving 'permanent' land cover conversion, and fires consuming peat soils can also result in a net release of carbon to the atmosphere, since unlike savannah or grassland fires the carbon released is not balanced by a roughly equivalent uptake over subsequent growing seasons (Sommers et al., 2014; Friedlingstein et al., 2020). Active fire (AF) remote sensing from space is a key technique used to deliver information on local to global scale fire activity for all these applications and more in a timely and accurate manner. Following a recent review of Earth Observation (EO) based burned area mapping (Chuvieco et al., 2019), here we focus on EO for active fires – a technique that has developed to now provide information on fire activity occurring anywhere on Earth with very low data latency and updates multiple times per day. Conducted as part of the Global Observation of Forest Cover/Global Observation of Landcover Dynamics (GOFC/GOLD) Fire

Programme (https://gofcgold.org/), this review summarizes the history of the AF remote sensing approach, details current capabilities and key applications, and identifies important developments deserving focus in the coming years. Appendix 1 provides a glossary and acronym list covering many of the terms used, along with a definition of some of the most relevant physical and chemical quantities.

Fig. 1 shows the annual distribution of actively burning landscape fires detected via processing of data collected by the Moderate Resolution Imaging Spectroradiometer (MODIS) instrument onboard NASA's Terra satellite. The fires detected include for example wildfires, those planned for some land management objective such as support to agriculture or forestry, and those used to clear land – including forests - for future agriculture. The data of Fig. 1 clearly illustrate that widespread landscape fire activity occurs on all continents except Antarctica, generally in regions with enough dry fuel and ignition sources from people or lightning. Globally an average of around 3.4% of Earth's terrestrial surface area burns annually (Giglio et al., 2018), an estimate that may increase as more finely detailed EO-derived burned area (BA) data become available (Roy et al., 2019; Roteta et al., 2019). Landscape fires such as these play important roles in many ecological (Bond and Keeley, 2005; McLauchlan et al., 2020) and wider Earth system processes (Bowman et al., 2009), including in relation to the carbon cycle (Sommers et al., 2014). But their annual consumption of billions of tonnes of vegetation and organic soil also results in globally significant emissions of smoke to the atmosphere (van der Werf et al., 2017), even
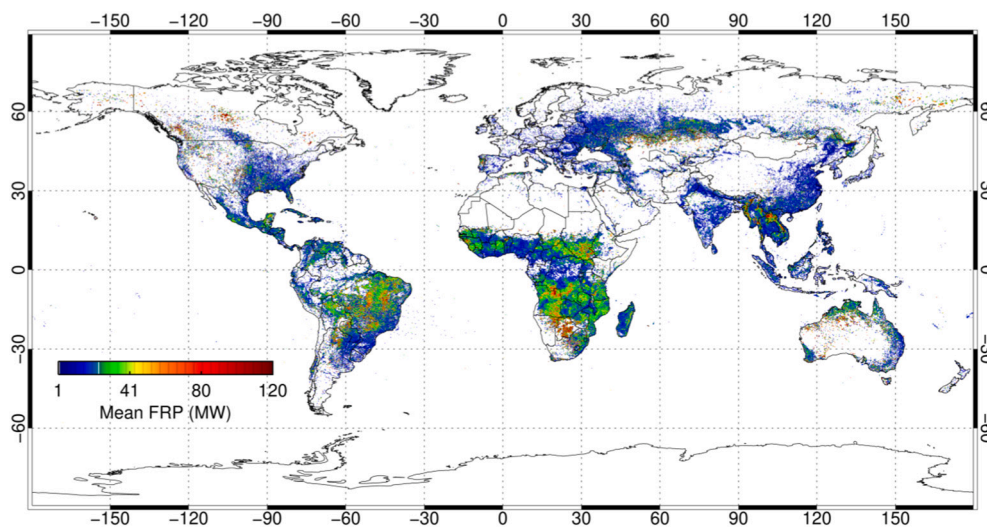

Fig. 1. One year of actively burning landscape fire radiative power (FRP), derived from MODIS observations made from the Terra satellite. Data are the mean FRP of all active fire pixels detected in each 0.5° grid cell, as defined by the MODIS MCD14ML Active Fire and Thermal Anomaly product generated for 2010 (Giglio et al., 2016).

from individual fire events (Hirsch and Koren, 2021), and this affects air quality (Jaffe et al., 2020) and human health (Roberts and Wooster, 2021). Those fires resulting in permanent landcover change, such as deforestation, and/or which consume carbon-rich organic soil such as peat built up over long-timescales also represent a net release of carbon to the atmosphere (e.g. Sommers et al., 2014; Huijnen et al., 2016) and so contribute to rises in atmospheric greenhouse gas concentrations. One of the earliest stimuli for use of satellite EO in studying landscape fires came from uncertainties on their net carbon budget impact (Seiler and Crutzen, 1980), though a century earlier von Danckelman had drawn attention to their role in large-scale aerosol radiative forcing (Brönnimann et al., 2009).

Satellite EO can be used to probe many fire characteristics, including burned area (Giglio et al., 2018; Chuvieco et al., 2019) and the concentration and composition of smoke plumes (e.g. Kaufman et al., 2002; Coheur et al., 2009; Ross et al., 2013). Active fire (AF) remote sensing such as that used to produce the data of Fig. 1 primarily focuses on identifying the location, timing and radiative strength (Fire Radiative Power; FRP) of fires that are actually consuming vegetation and/or organic soil at the time the observations were made. The FRP is somewhat akin to a spatial integration of the intensity of the overall combustion zone, and is measured in Watts. AF remote sensing is based primarily on infrared (IR) spectral measurements, and we begin by summarizing the historical development of the approaches used to exploit these measures (Section 2). We then review the fundamental physics (Section 3) and strategies for AF detection (Section 4), detailing approaches for FRP retrieval and the extraction of related variables such as fire effective temperature and area (Section 5). We examine how such data relate to fuel consumption and atmospheric impacts (Section 6), fire characteristics and ecosystem variables (Section 7), and how they are increasingly provided via online portals and in 'analysis ready' formats (Section 8). Finally, to aid future planning, we examine types of sensors, datasets and research activities we consider important for further development of AF applications, so as to point the way to areas of further fruitful research (Section 9).

2. The historical development of satellite active fire (AF) methods

The origins of active fire remote sensing extend back to 1960's and 1970's, with airborne thermal imaging of forest and coal seam fires (e.g. Hirsch, 1965; Ellyett and Fleming, 1974). Satellite-based studies commenced in the early 1980's, primarily using data from the Advanced Very High Resolution Radiometer (AVHRR) operating onboard NOAA's Polar-orbiting Operational Environmental Satellites (POES). AVHRR data played a key role in the development of AF detection methods (e.g., Flasse and Ceccato, 1996; Giglio et al., 1999; Ichoku et al., 2003). Research was largely based on the strong 'active fire sensitivity' of spectral bands located in the middle infrared (MIR) atmospheric window (3–5 μm) (Section 3), with the AVHRR 3.7 μm channel shown to discriminate areas of combustion covering <1% of the pixel area (Dozier, 1981; Matson and Dozier, 1981; Muirhead and Cracknell, 1985; Flannigan and Vonder Haar, 1986; Lee and Tag, 1990; Setzer and Pereira, 1991; Justice et al., 1993). The sensitivity of MIR measurements to sub-pixel thermal anomalies still underpins most AF remote sensing today, and AVHRR itself is still used (e.g., in the Brazilian 'Queimadas' fire monitoring system described in Appendix 2). During the 1980's the first AVHRR-based active fire initiatives were unable to use the full spatial resolution (1 km) data globally due to the limited 'local area coverage' (LAC) onboard storage capacity of POES. However, a global network of AVHRR ground stations collected the directly downlinked High Resolution Picture Transmission (HRPT) 1 km data broadcast from the POES within their coverage areas, and in 1992 the International Geosphere Biosphere Programme Data and Information System (IGBP-DIS) provided specifications for the first global 1 km data set (Eidenshink and Faundeen, 1994). This led to the first ever day and night

global AF data set, produced by Europe's Joint Research Center (JRC; Ispra) covering April 1992 to December 1993 (Stroppiana et al., 2000). The nighttime only ESA World Fire Atlas (WFA) was developed at a similar time using initially ATSR-2 observations (Arino et al., 1999). The call for such global fire products originated in the requirements set by the IGBP Global Change and Terrestrial Ecology (GCTE) Core Project and the response by IGBP Data and Information Systems (IGBP-DIS), and was taken up more comprehensively by the international community through the GOFC/GOLD program (Ahern et al., 2001; Csiszar et al., 2013). Most recently the nearly 40-year archive of global, lower (~ 3 × 5 km) spatial resolution subsampled AVHRR global area coverage (GAC) data has been mined to generate some of the longest AF records currently available, initially regionally (e.g. Wooster et al., 2012a) and now being extended globally. Fig. 2 shows an example of a three-decade AVHRR-GAC AF analysis of southern Canadian provinces (Fig. 2a), where extreme fires burned in Manitoba in May, July and August 1989 (Fig. 2b).

Work with AVHRR fundamentally changed our understanding of the global presence of fire, but the low sensor saturation temperature (c. 325 K) of AVHRRs 3.7 μm MIR band (Csiszar and Sullivan, 2002), significant POES orbital drift (Csiszar et al., 2003) as well as other issues (Giglio and Roy, 2020) provided limits to its utility. However, such work greatly influenced the presence of an AF detection and characterization capability within NASA's Earth Observing System (EOS; Justice et al., 1998), specifically that of the EOS flagship sensor - MODIS (Justice et al., 2002a). MODIS was designed with two 3.96 μm MIR channels having different saturation temperatures and dynamic ranges to support FRP retrieval as well as AF detection (Kaufman et al., 1998; Justice et al., 2002b). FRP retrieval (Section 5) enables the AF application to go beyond fire presence/absence mapping to quantify the amount of radiant energy a fire is emitting per unit time, which is now considered linearly related to rates of fuel (vegetation and/or organic soil) consumption and smoke emission (e.g. Kaufman et al., 1996; Ichoku and Kaufman, 2005; Wooster et al., 2005; Kaiser et al., 2012; Nguyen and Wooster, 2020). The MODIS AF detection algorithms were built on the AVHRR experience and prototyped using MODIS airborne simulator data (Kaufman et al., 1998). They exploited the increased brightness temperature (BT) difference found between the MIR and long-wave infrared (LWIR) channel measurements at pixels containing actively burning fires (Section 3). The MODIS AF detection algorithm (Section 4) has been used by NASA to generate a suite of AF products having better than daily temporal resolution since the year 2000, and these remain to the present time one of the most widely used MODIS products. Other satellites in the 1990's and 2000's also supported AF detection, including the Defense Meteorological Satellite Program nighttime low-light imaging Operational Linescan System (DMSP-OLS) (e.g. Cahoon Jr et al., 1992; Elvidge et al., 2013) and the Tropical Rainfall Mapping Mission (TRMM) which relied on evolutions of AF detection methods first used with AVHRR (e.g. Giglio et al., 2000).

AF detection accuracy assessment is challenging due to the ephemeral and highly dynamic nature of landscape fire, difficulties in obtaining independent reference data coincident with the satellite observations, and because surface fires are complex to characterize in situ. However, for MODIS, the inclusion of the higher spatial resolution (15, 30 and 90 m) Advanced Spaceborne Thermal Emission and Reflection Radiometer (ASTER) instrument operating concurrently on the Terra satellite and itself able to be used for AF detection enabled simultaneous reference data to be collected. A systematic evaluation of the minimum fire sizes detectable by MODIS was produced (Morisette et al., 2005; Schroeder et al., 2008), and further refinements to the MODIS AF detection algorithm were informed by this validation. This culminated in the latest Collection 6 dataset reprocessing (Giglio et al., 2016). These developments also influenced algorithms used with subsequent low earth orbit (LEO) satellite sensors, such as the Visible Infrared Imaging Radiometer Suite (VIIRS) (Csiszar et al., 2014) and Sentinel-3 Sea and Land Surface Temperature Radiometer (SLSTR)
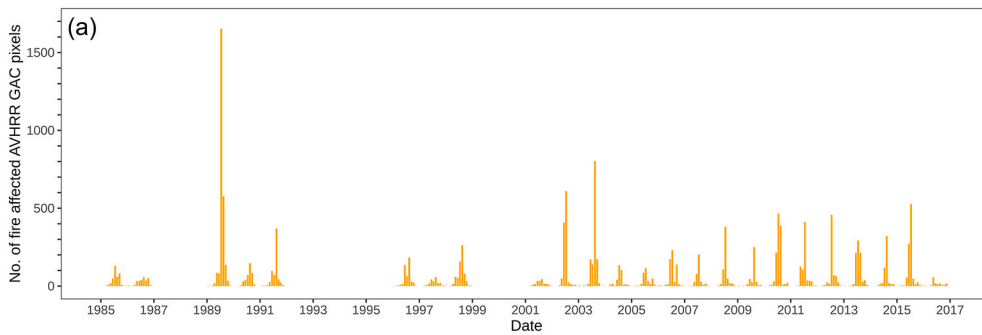
Fig. 2. Example of (a) long term and (b) extreme landscape fire activity recorded in southerly Canadian provinces, as depicted via analysis of AVHRR GAC data. (a) AF detection time series derived using night-time GAC data from 1985 to 2016. (b) Example AVHRR GAC image of 24th July 1989 (09:00 UTC) taken during the extreme 1989 Manitoba fire season (see the peak in (a) and Hirsch, 1991). Cloudy pixels are masked as grey and active fire pixels shown by the high MIR (3.7 μm) channel brightness temperature elevation over the ambient background (red areas). (For interpretation of the references to colour in this figure legend, the reader is referred to the web version of this article.)
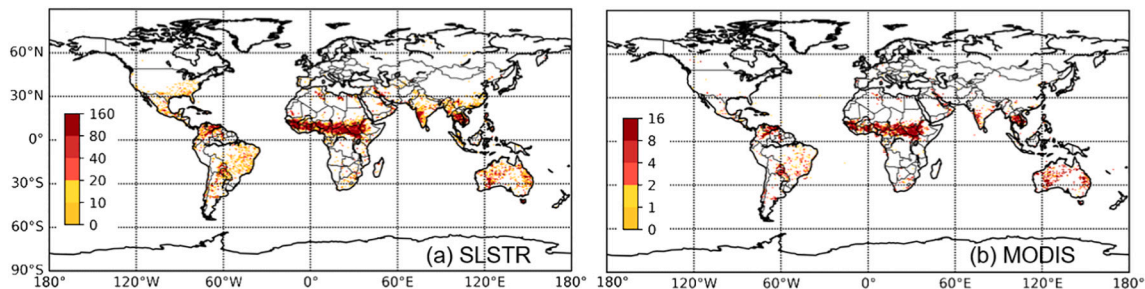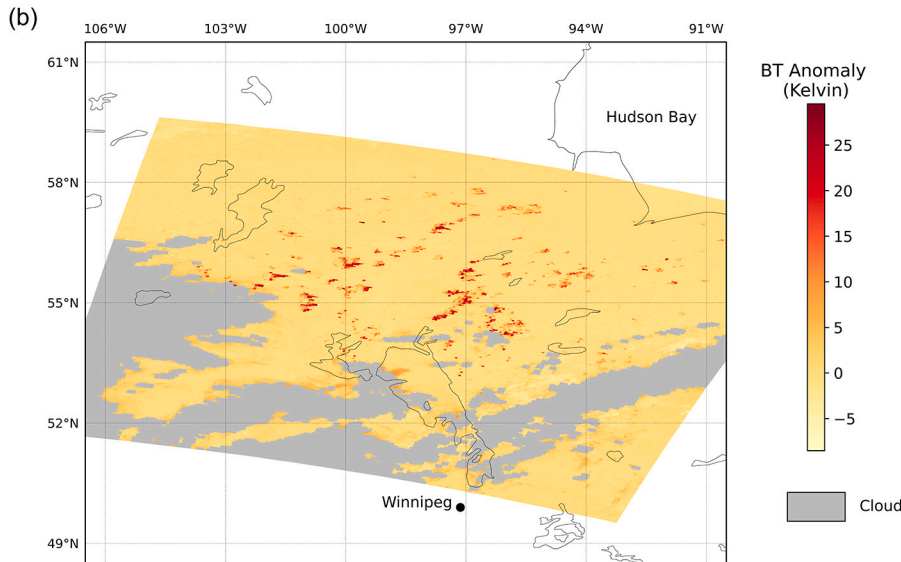

Fig. 3. Nighttime active fire pixel counts detected in 0.1° grid cells in January 2019 from (a) Sentinel3B SLSTR and (b) Terra MODIS. These sensors have similar local overpass times and show similar spatial patterns of AF detection, but the SLSTR data record shows far higher AF pixel counts. Analysis shows this is in part due to the detection of many lower FRP fires by SLSTR than MODIS. This is a result of the former sensors smaller pixel area growth around the swath compared to MODIS (Wooster et al., 2012a; Xu et al., 2020), and the fact that lower FRP fires are typically the most numerous (e.g. Wooster and Zhang, 2004).

(Wooster et al., 2012b; Xu et al., 2020). Inter-comparisons of AF data derived from observations made by different LEO sensors are commonly used to understand their varying performance characteristics (Fig. 3), with one aim being to derive transfer functions enabling data from multiple sensors to be combined into single time-series.

A similar AF detection algorithm development cycle has occurred for geostationary (GEO) satellite AF products as with LEO products. Compared to LEO systems, GEO products offer higher temporal resolutions but coarser spatial resolutions, and each sensor only provides data over a specific region of the Earth (Fig. 4). Geostationary AF products were first generated over the America's using the Geostationary Operational Environmental Satellite Visible Infrared Spin Scan Radiometer Atmospheric Sounder (GOES-VAS) (e.g. Prins and Menzel, 1992, 1994; Weaver et al., 1995), and this led to the development of the long-standing GOES WildFire Automated Biomass Burning Algorithm (GOES WFABBA) product (Prins et al., 1998). The GOES WFABBA products represent the longest geostationary AF dataset currently available, and in addition to AF location and time included an estimate of effective AF temperature and area - derived using the Dozier (1981) 'bi-spectral' approach (Section 4). Wooster et al. (2005) and Roberts et al. (2005) first demonstrated the retrieval of FRP from geostationary EO data, doing so via an approach avoiding use of bi-spectral data (see Section 5), and went on to develop a full 'fire thermal anomaly' (FTA) AF detection and FRP retrieval algorithm for GEO systems. This was first
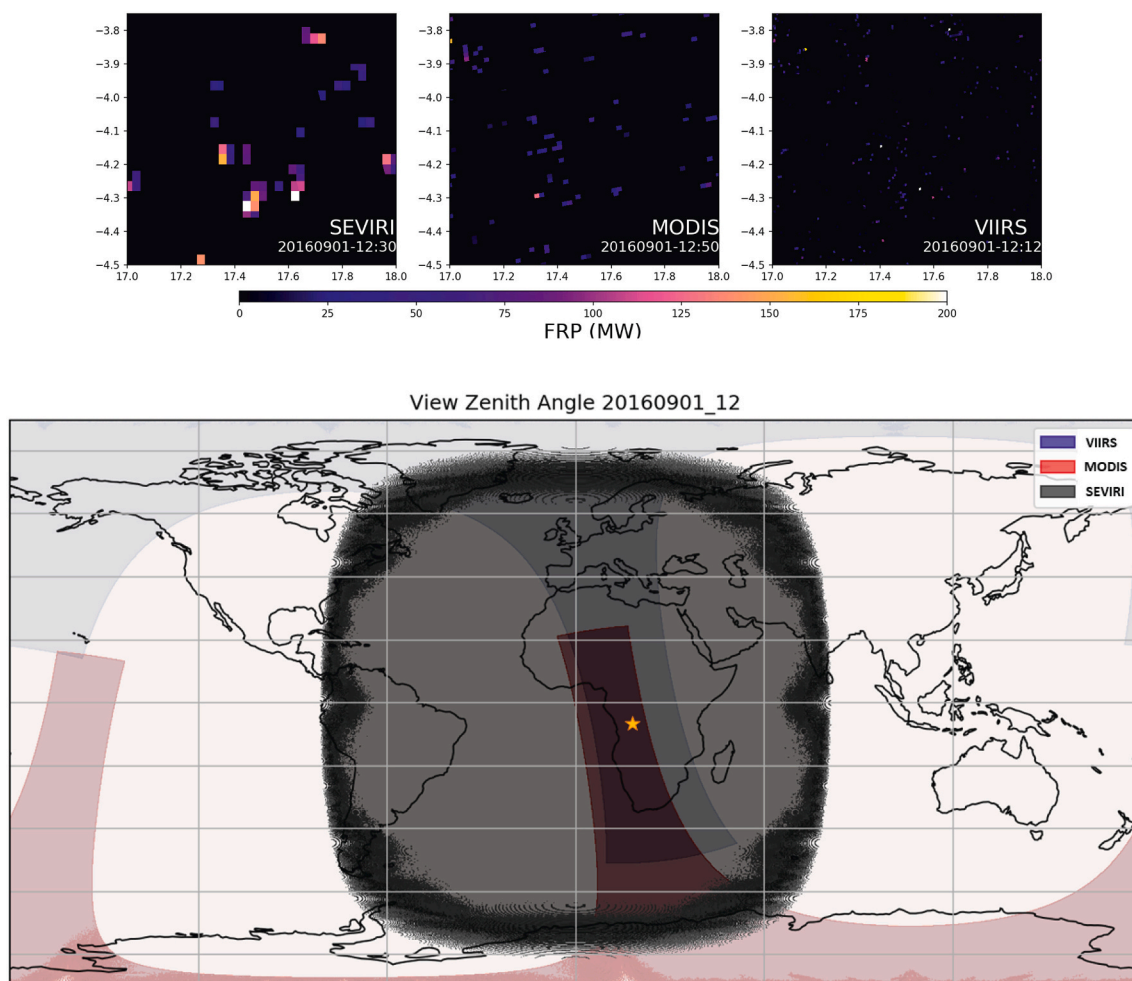
Fig. 4. Active fire data and coverage maps derived from observations made by the geostationary Meteosat Second Generation SEVIRI instrument (SEV), and the polar-orbiting Aqua MODIS (MYD) and VIIRS (VNP) at approximately the same time of day. An approximately 80 × 100 km region of southern Africa is shown at top, where the coarser spatial detail of SEVIRI is apparent but also the higher per pixel FRP values due to the capturing of more fires within a pixel. The spatial coverage of each of these systems obtained in a single hour is shown in the global map, with the location of the focus region highlighted. (For interpretation of the references to colour in this figure legend, the reader is referred to the web version of this article.)

applied to data from Meteosat Second Generation (Roberts and Wooster, 2008), and an operational version is now used to generate a series of geostationary AF detection and FRP retrieval products spanning much of the globe, including from Meteosat over Africa and Europe (Wooster et al., 2015), GOES-East and -West over the America's (Xu et al., 2010; 2021) and Himawari over Asia (Xu et al., 2017). Similar product intercomparisons and evaluations have been conducted as for LEO AF products (e.g. Roberts et al., 2015).

3. Basic physics of active fire remote sensing

AF detection and characterization is based on remote sensing of some of the approximately 20 MJ.kg^{-1} of energy released when vegetation and organic soil burns (Cheney and Sullivan, 2008). 'High heat of combustion' describes the maximum total energy release per unit of dry matter consumed, and so live, i.e., moist, fuels release somewhat less (Smith et al., 2013). Of the total energy released, only about 10–20% is released as (primarily IR) electromagnetic radiation (Freeborn et al., 2008; Kremens et al., 2012). This radiative energy release rate is far higher than from the same area of ambient land however, and its spectral distribution follows Planck's Radiation Law and its derivative Wien's Displacement Law which serve as the physical basis for most AF remote sensing.

Fig. 5 shows the modelled blackbody emitted spectral radiance for

surfaces at 300 K, 600 K and 1000 K (typical temperatures of the Earth's land surface, smoldering, and flaming combustion respectively; Kaufman et al., 1998; Sullivan et al., 2003; Dennison et al., 2006). The emitted spectral radiance from a 1000 K flaming fire in the longwave IR (LWIR) atmospheric window (8–14 μm) is more than an order of magnitude higher than from the ambient land surface, but in the MIR (3–5 μm) atmospheric window it is almost three orders of magnitude higher – demonstrating why MIR observations are so sensitive to the presence of actively burning fires. Cooler smoldering fires show lower but still very significant levels of MIR and LWIR emittance. The very strong radiative signal of areas of combustion in the MIR spectral region, and the contrast between this and that seen in the LWIR from the same location, and in the MIR from nearby ambient non-fire areas, mean that active fires can be detected in appropriately remotely sensed imagery even if they cover an extremely small fraction of a pixel.

To demonstrate that even small sub-pixel fires generate very detectable changes in the signal of the pixels they are contained within, Fig. 6 shows an example of modelled top-of-atmosphere (TOA) spectral radiance for different pixel situations, fully taking into account both emitted and reflected radiation and atmospheric effects. The figure contrasts a 300 K savannah land surface pixel (green line) with the same pixel but also containing 0.5% areal coverage of flaming 1000 K combustion (red line). In the MIR spectral region (3–5 μm), there is around an order of magnitude difference between the spectral radiance of these
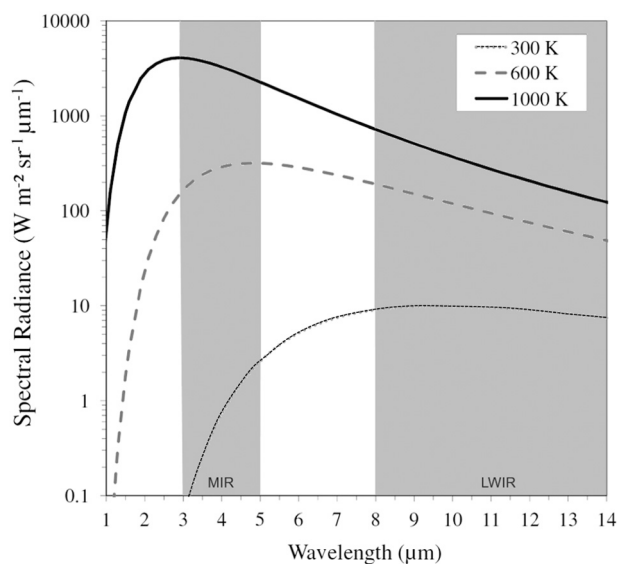
Fig. 5. Emitted spectral radiance for blackbodies at typical flaming (1000*K*) and smoldering (600 K) temperatures along with that from an ambient 300 K surface. Note the logarithmic scale of the y-axis. The MIR and LWIR atmospheric window regions are shaded grey.
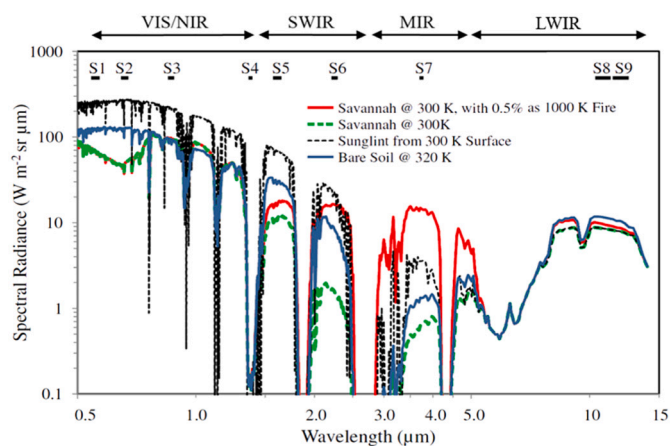
Fig. 6. Modelled top-of-atmosphere emitted spectral radiance for four pixels – containing ambient (300*K*) savannah; the same but with a 1000 K actively burning fire covering 0.5% of the pixel area, specularly-reflected sunglint from a 300 K surface, and solar-heated bare soil at 320 K. Examples of typical spectral bands of a satellite based imaging radiometer used to detect AF pixels are shown at top (here those from the Sentinel-3 SLSTR sensor; Wooster et al., 2012a). Savannah pixels which contain a sub-pixel active fire are best separated from non-fire pixels in MIR spectral region, which is targeted by the SLSTR S7 spectral band. SLSTR also has a second (low-gain) MIR band (F1) to avoid saturation effects that impact S7 over warmer areas and active fires (see Section 10).

two pixels, equivalent to an easily detectable brightness temperature (BT) difference of around 80 K - even though the fire covers less than 1% of the pixel area. Whilst there is a dependency on issues such as day/night operation, and certain instrument-specifics, most AF detection algorithms can identify pixels in remotely sensed imagery that contain active fires if they have induced a minimum 5 to 10 K increase in the pixels MIR brightness temperature compared to the non-fire background. As such, fires covering down to perhaps ~0.01% of the pixel area are potentially identifiable. A far lower (but still likely detectable) signal difference between the fire and non-fire savannah pixels is apparent in the 10–12 μm LWIR spectral region of Fig. 6, indicating that

fires essentially have to cover a far larger portion of the pixel area to be identified using LWIR observations than MIR observations. These types of spatial and spectral contrast differences are the basis of most AF detection algorithms, with various additional tests employed to discriminate AF pixels from 'false alarms'. Pixels containing homogeneously warm (e.g. solar heated) land would be expected to have more similar MIR and LWIR BTs than would AF pixels, enabling the latter to be discriminated using this characteristic (see Section 4), whilst geographic masks can be used to screen out land-based gas flaring and active volcanoes for example.

Fig. 6 also shows the signal of a pixel containing sunglint over water, which is a key cause of potential false alarms since sunglint affected pixels can have similar MIR and LWIR signals to AF pixels. However, sunglints can be masked out based on their typically strong visible wavelength and/or near infrared (NIR) signals (e.g. Zhukov et al., 2006). Sunglint does not occur at night, and so nighttime AF detection algorithms can often be deployed with increased sensitivity, including because nighttime ambient surface temperatures are typically lower and more homogeneous than by day - leading to potential increases in the contrast provided by AF pixels. Some nighttime AF detection algorithms employ analysis of short-wave infrared (SWIR) signals (typically between 1.6 and 2.2 μm), which Figs. 5 and 6 shows are also raised by the presence of sub-pixel active fires. By day however such emitted SWIR signals can be masked by variations in solar reflected radiation unless the fire covers a substantial fraction of the pixel area. Such methods are thus best suited to use with higher spatial resolution imagery (e.g. Giglio et al., 2008).

Few active fires completely fill a satellite image pixel, and extremely rarely at the scale of MODIS, SLSTR and VIIRS pixels. Thus subpixel AF situations such as is modelled in Fig. 6 are by far the most common type. However, reliable detection of extremely small subpixel (e.g. < 0.01% pixel area), sub-canopy smoldering, or particularly cool (e.g. subsurface peat) fires remains a challenge. A fire of a given size and temperature will also occupy a smaller areal fraction of a larger pixel than a smaller pixel, reducing its detection reliability. However, moderate spatial resolution EO data such as provided by AVHRR, MODIS, VIIRS, and SLSTR are available with a daily or better update frequencies, enabling detection of active fires covering around 100 m^2 and in some cases even smaller (Schroeder et al., 2014; Zhang et al., 2017). Fig. 7 shows an AVHRR 1 km image captured over Indonesia during a period when flaming vegetation fires and cooler (often sub-surface) smoldering peat fires were widespread. These fires are generally strongly sub-pixel in size, and in agreement with Figs. 5 and 6 their influence on the MIR BT image (a) is far greater than in the LWIR BT image (b). The BT difference image (Fig. 7c) best highlights the AF pixels, and this difference metric is the basis of most AF detection algorithms (Section 4).

Fig. 7 shows a largely cloud free situation. Unlike smoke, meteorological clouds obscure active fires from view, and can also contribute to sunglint-induced false alarms. Cloud masking is thus an important component of EO-based AF detection. Information on cloud masked areas is also essential for AF product users to understand whether a location is considered free of detectable fires, or whether there is uncertainty due to cloud cover. Atwood et al. (2016) demonstrate that AF detection can occur through even very thick smoke, but that some satellite AF product cloud masking procedures inadvertently mask out heavily smoke affected areas as being affected by cloud. Conservative cloud masks can also result in higher rates of AF omission, and so underestimation of regional-scale FRP totals (Freeborn et al., 2014b; Hall et al., 2019; Liu et al., 2020). However, Wooster et al., (2018) demonstrate that considerable spatio-temporal detail on fire activity in strongly smoke and cloud affected regions can still be gained with suitable tailoring of AF product cloud masking procedures.

To aid understanding of the exact source of the types of elevated spectral signals shown in Fig. 6 over fire affected pixels, Parent et al. (2010) made high spectral resolution laboratory measurements of fire emitted radiation. Planckian thermal emission was seen coming from
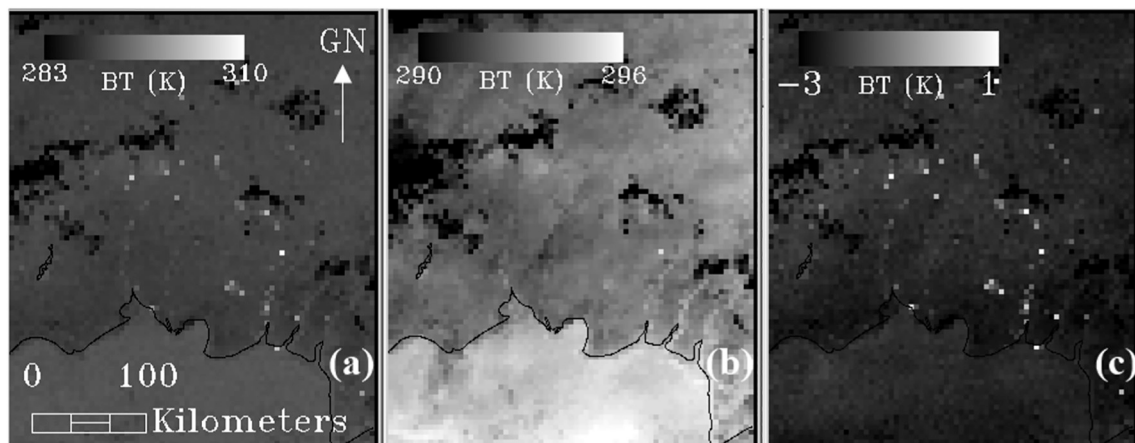
Fig. 7. Night-time AVHRR local area coverage (LAC) ~ 1 km spatial resolution imagery of large-scale fires burning in primarily in peatlands across southern Kalimantan (Indonesia) on 24th August 1991. (a) MIR and (b) LWIR brightness temperature (BT) data. The presence of a sub-pixel fire affects the BT more in the MIR than in the LWIR, and the MIR and LWIR BT difference shown in (c) most clearly highlights them.

both the hot fuel and from luminous hot soot particles in the flames, but whilst the fuel typically had a high emissivity across the IR region, that of the flames depended strongly on soot concentration and flame depth (Àgueda et al., 2010; Johnston et al., 2014). However, even in low emissivity (e.g. thin, low soot concentration) flames showing low amounts of Planckian thermal emission, strong thermal emission in narrow spectral 'emission line' regions were seen from hot gases such as CO_2 and H_2O (Parent et al., 2010). EO sensors prioritized for AF remote sensing generally avoid use of such spectral regions however, since ambient atmospheric CO_2 and H_2O absorb strongly at these same wavelengths and would tend to obscure the surface emitted signals when observing from space. Atmospheric transmittance is taken into account of during the generation of certain AF products, but typically only in terms ambient atmospheric gaseous constituents (e.g. Wooster et al., 2015; Section 5). In terms of aerosols, wildfire smoke is dominated by very small particles (i.e. PM2.5 and smaller) that are inefficient scatterers of MIR and LWIR radiation, and this is the reason that fires can be identified though even strongly smoke-affected regions as long as the data are not masked as cloudy (Atwood et al., 2016). However, thick smoke is likely to have some impact on the retrieved FRP, including via any black carbon component absorbing some of the fire-emitted thermal radiance. This is yet to be accounted for in FRP retrieval algorithms.

4. Active fire detection algorithms and products

4.1. Active fire detection algorithms

4.1.1. Early work

Dozier (1981) and Matson and Dozier (1981) undertook some of the earliest satellite-based studies of sub-pixel 'thermal anomalies'. They explained the causes of the spectrally varying BTs seen in AVHRR data containing sub-pixel hot sources (e.g. Fig. 7), and these characteristics still underly almost all AF detection methods used today. They proposed a so-called bi-spectral fire characterization algorithm that used non-linear simultaneous equations to estimate the fires sub-pixel effective temperature and area (see Section 5.1). Prior to application of this bi-spectral, other approaches are often used to identify the pixels to which it should be applied.

4.1.2. Fixed threshold algorithms

Fixed threshold AF detection algorithms apply relational operators and fixed thresholds to the BT data captured in individual spectral bands (e.g., $T_{MIR} > 320$ K) and/or to band differences (e.g., $T_{MIR} - T_{LWIR} > 10$ K). Their simplicity provides computational efficiency, but even carefully-tuned thresholds can in general only satisfy AF detection

accuracy requirements under the specific regional/seasonal conditions for which they were derived (Kaufman et al., 1990; Pereira and Setzer, 1993), or they must be applied under relatively stable ambient background temperature conditions (e.g. at night; Wooster et al., 2012b). Use of higher thresholds can help alleviate false alarms related to by ambient background temperature variations, as was the case with the ESA World Fire Atlas, but increase the chance of omitting smaller and/or cooler fires (Arino et al., 1999).

4.1.3. Contextual algorithms

Contextual algorithms incorporate dynamic thresholds, which adapt to local conditions to aid detection of smaller and/or cooler fires whilst minimizing false alarms. In this approach, candidate AF pixels are first detected using liberal fixed thresholds - generally applied to the T_{MIR} and/or $T_{MIR} - T_{LWIR}$ data. False detections are then removed from this 'potential AF pixel' set by comparing the signal of each candidate AF pixel to that of neighboring non-fire pixels within a surrounding geographic window. Some of the first contextual AF detection algorithms were developed for use with AVHRR (e.g. Flasse and Ceccato (1996); Giglio et al., 1999) as part of the IGBP-DIS global fire initiative (Section 2). Evolutions followed, including use of differently sized windows (e.g. Giglio et al., 2003, 2016; Zhukov et al., 2006), and spatial filters to improve rejection of non-fire pixels in the early stages and allow use of more liberal fixed thresholds able to better capture smaller/cooler fires (Roberts and Wooster, 2008).

Contextual algorithms still remain the most commonly used AF detection method. Since their initial development (Flasse and Ceccato, 1996; Giglio et al., 1999; Kaufman et al., 1998), they have been applied to data from numerous LEO sensors, including VIIRS (Schroeder et al., 2014; Csiszar et al., 2014; Zhang et al., 2017), MODIS (Kaufman et al.,1998; Giglio et al., 2016), the BIRD Hot Spot Recognition System (HSRS, Zhukov et al., 2006), the TRMM Visible and Infrared Scanner (VIRS, Giglio et al., 2000), SLSTR (Wooster et al., 2012b; Xu et al., 2020), and Landsat (Schroeder et al., 2016; Kumar and Roy, 2018), and also GEO sensors such as those carried by Meteosat (e.g. Wooster et al., 2015; Amraoui et al., 2010; Di Biase and Laneve, 2018), GOES (Prins et al., 1998; Xu et al., 2010; Schmit et al., 2017; Xu et al., 2021a), Himawari (Xu et al., 2017; Wickramasinghe et al., 2016), and FengYun (Xu et al., 2010).

4.1.4. Multi-temporal algorithms

The majority of AF detection algorithms are applied to single date imagery, with some adding basic temporal constraints to remove possible false alarms (e.g., Prins et al., 1998; Xu et al., 2010; Kumar and Roy, 2018). Some multi-temporal AF detection algorithms have been

developed however. These either identify fire-related pixel-level thermal variations via multi-temporal change detection (e.g. Filizzola et al., 2017), or model the ambient pixel BT diurnal cycle and identify fire-related departures from this (e.g. Roberts and Wooster, 2014). Both approaches aim to identify an AF pixel via thermal differences compared to expectations, whilst accounting for temporal variability. In the multi-temporal change detection approach, statistical characterizations of a fire-relevant parameter (e.g., the MIR BT or MIR-LWIR BT difference) at each pixel location are calculated over a suitably long period; and such approaches have been applied to LEO (Marchese et al., 2017) and GEO (Laneve et al., 2006; Filizzola et al., 2017) data. Model-based approaches exploit the latter's higher temporal frequency to characterize the ambient BT diurnal cycle and then forecast this forward in time (Udahemuka et al., 2007; Hally et al., 2017). Optimal estimation techniques, such as Kalman filters, can build on this baseline to assimilate observed BTs and deploy statistical thresholds to confirm whether active fires are present based on departures from the modelled diurnal trend. Although computationally intensive, this approach has been applied to GEO data (van den Bergh and Frost, 2005; van den Bergh et al., 2009; Roberts and Wooster, 2014; Hally et al., 2017), and in some cases has been shown to detect fires unidentifiable using the more standard contextual approach (van den Bergh et al., 2009; Roberts and Wooster, 2014).

4.1.5. Non-thermal infrared methods

AF detection methods using visible (VIS), NIR and SWIR band data have been developed for nighttime use. The VIS-NIR band (0.5–0.9 µm) on the 2.7-km U.S. Air Force DMSP-OLS sensor (Elvidge et al., 1996) enabled nighttime detection of city lights, lightning flashes and active fires using a simple contextual algorithm that identified pixels far brighter than its neighbors. Elvidge et al. (2013) extended the approach to 750 m VIIRS day-night band (0.5–0.9 µm) data, combining it with that from the SWIR-to-LWIR bands and using a Planck function fitting approach to more confidently discriminate fires from other visible light sources. Some nighttime AF detection algorithms also employ SWIR radiances measures where available. For example, Elvidge et al. (2015) combined Landsat-8 SWIR and LWIR data to discriminate flaming and smoldering peatland fires, whilst Fisher and Wooster (2019) used nighttime SLSTR SWIR and MIR data to discriminate gas flares from vegetation fires.

Daytime SWIR algorithms have also been developed for use with medium spatial resolution sensors having no MIR capability. The most common approaches, developed for ASTER (Giglio et al., 2008) and then Landsat-8 (e.g., Schroeder et al., 2016; Kumar and Roy, 2018) rely on a fire-sensitive SWIR band and a comparatively insensitive NIR band to identify the increased SWIR radiance associated with fires (Fig. 6). Commission errors can result from some highly reflective non-burning surfaces (e.g., certain buildings), but the joint availability of Landsat-8 and Sentinel-2 imagery provides ~3-day median global coverage (Li and Roy, 2017) and the potential for relatively infrequent but spatially detailed global AF detection.

Finally, more experimental techniques requiring still novel sensors have been developed. For example, the identification of specific narrow-band NIR emission lines related to the thermal excitation of potassium (K) that occurs only in flaming fires has seen an early demonstration from space (Amici et al., 2011).

5. Fire radiative power (FRP) and fire characterization

5.1. FRP retrieval

Since the late 1990's, AF detections have been increasingly accompanied by efforts at fire characterization, mostly in terms of retrievals of fire radiative power (FRP; usually expressed in MW). FRP is the rate at which the fires within a pixel are emitting thermal energy, integrated over all angles and wavelengths. An empirically-derived algorithm for

direct estimation of FRP was first proposed and demonstrated with MODIS airborne simulator data by Kaufman et al. (1998) - Eq. (1). An underlying assumption is that, since heat yields are relatively constant among vegetation types (Stott, 2000), remotely sensed FRP retrievals provide data useful for estimating rates of fuel consumption and smoke emission, as first demonstrated by Wooster et al. (2005) and Kaufman et al. (1998), Freeborn et al., (2008) and Ichoku et al. (2008) respectively. Eq. (1) was used to retrieve FRP in the early (Collections 1–4) MODIS AF Products (Giglio et al., 2003), in units of emitted power per unit area of the pixel:

$$FRP = 4.34 \times 10^{-19} \sum \left(T_{MIR,fire}^8 - T_{MIR,bg}^8 \right) \tag{1}$$

where $T_{MIR,\ fire}$ and $T_{MIR,\ bg}$ are the MIR BT (K) of the AF pixel and the mean of the surrounding "background" pixels respectively.

Whilst Eq. (1) performs well for MODIS, its empirical nature means it is specific to data from that sensor. It starts to underperform when applied to finer spatial resolution data that record higher BTs due fires covering a greater proportion of their pixel area (Section 3) (Wooster et al., 2003). Wooster et al. (2003, 2005) derived a more physically based approach to FRP retrieval, based on a power-law approximation to the Planck function and which linearly related FRP (MW) to the AF pixels excess MIR spectral radiance above the background:

$$FRP = \frac{A_{sampl}.\sigma.\varepsilon}{.\varepsilon_{MIR}} \left(L_{MIR,fire} - L_{MIR,bg} \right) \tag{2}$$

where σ is the Stefan-Boltzmann constant (5.67×10^{-8} J s^{-1} m^{-2} K^{-4}) and ε and ε_{MIR} are the broadband and MIR spectral emissivities respectively (that cancel as the fire is generally considered a greybody or blackbody), L_{MIR} is the MIR spectral radiance of the AF pixel (W m^{-2} sr^{-1} µm^{-1}), and $L_{MIR,\ bg}$ is the estimate of what the AF pixel spectral radiance would be if it did not have a fire within it (typically taken as the mean or median MIR spectral radiance of the surrounding background pixels), α (W m^{-2} sr^{-1} µm^{-1} K^{-4}) is a coefficient dependent upon the sensor's MIR channel spectral response (Wooster et al., 2005), and A_{sampl} is pixel area (km^2).

Similar to its use in Eq. (2), for MODIS Collection 5 an A_{sampl} multiplier was added to Eq. (1) to provide MODIS FRP outputs directly in MW, and from Collection 6 onwards the FRP retrieval method was shifted to Eq. (2) (Giglio et al., 2016). Giglio et al. (2016) found an average 16% difference when comparing MODIS' FRP retrievals based on Eqs. (1) and (2), with greater differences at lower FRPs reflecting the fact that the MIR radiance method tends to underestimate FRP for emitters <600 K (a lower temperature than that of most active combustion zones; Wooster et al., 2003; Dennison et al., 2006). This underestimation is not necessarily disadvantageous, since it means that radiant heat from warm, recently burned areas not actively consuming fuel often do not contribute significantly to the total per-pixel FRP measure from which combustion rates are often derived (Wooster et al., 2005). However, it may prove more problematic in peatland fires, where underground combustion can lead to rather low surface temperatures in the burning areas (e.g. Elvidge et al., 2015; Fisher et al., 2020).

Moving beyond the single-band FRP retrieval methods discussed above, another approach to FRP estimation is to exploit outputs of the 'bi-spectral' method introduced in Section 4.1.1, namely the effective fire temperature (T_f, K) and sub-pixel proportion (p_f) of the Matson and Dozier (1981) and Matson and Holben (1986) approach:

$$L_{MIR} = \tau_{MIR} p_f B_{MIR}(T_f) + (1 - p_f) L_{MIR,bg} \tag{3}$$

$$L_{LWIR} = \tau_{LWIR} B_{LWIR}(T_f) + (1 - p_f) L_{LWIR,bg} \tag{4}$$

$$FRP = \sigma \left(T_f^4 - T_{bg}^4 \right) p_f A_f \tag{5}$$

where L_x is the AF pixel spectral radiance (W m^{-2} sr^{-1} µm^{-1}) observed

in the denoted spectral band x, $B_x(T)$ is the Planck function (W m^{-2} sr^{-1} μm^{-1}), τ is the atmospheric transmittance, $L_{X,\,bg}$ is the ambient background spectral radiance (i.e. non-fire, W m^{-2} sr^{-1} μm^{-1}), σ is the Stefan-Boltzmann constant (5.67×10^{-8} J s^{-1} m^{-2} K^{-4}) and $T_{x,\,bg}$ is the brightness temperature (K) of the ambient background in band x.

Per-pixel errors of T_f and p_f can be large, especially for lower values of p_f, and errors of ~100 K and ± 50% respectively at one standard deviation (σ_η) were demonstrated for even easily detectable active fires (p_f >0.005; or 0.5% of the pixel area) by Giglio and Kendall (2001). This is mainly due to challenges in sufficiently precisely isolating the difference between the AF and ambient background pixel signals in the LWIR - where fire thermal emission is far less strong (Figs. 5, 6 and 7), though errors in T_f and p_f may counteract each other somewhat when delivering FRP through Eq. (5) (Wooster and Rothery, 1997). Inter-band spatial misregistration effects can also impact bi-spectral estimation of T_f and p_f (Shephard and Kennelly, 2003), though Briess et al. (2003) and Zhukov et al. *(*2006*)* tackled this by applying the approach at the fire cluster (rather than AF pixel) level. Overall, whilst the geostationary GOES WFABBA product (Prins et al., 1998) applied this approach for FRP estimation, it is not particularly recommended for use with moderate to low spatial resolution data (Giglio and Schroeder, 2014; Giglio and Kendall, 2001). Most LEO and GEO AF products now base their per-pixel FRP retrievals on the MIR radiance method of Eq. (2) (Wooster et al., 2003, 2005). This includes those from VIIRS (Csiszar et al., 2014), Meteosat (Wooster et al., 2015), Himawari (Xu et al., 2017), GOES (Xu et al., 2010; 2021), SLSTR (Xu et al., 2021a, 2021b) and MODIS (Giglio et al., 2016).

In 2020, the Committee on Earth Observation Satellites (CEOS) Land Product Validation (LPV) Subgroup indicated that the current validation level of satellite FRP products is less advanced than for burned area, partly due to the ephemeral nature of active fires and the logistical and technical difficulties posed when trying to get independent, simultaneous FRP observations to match satellite estimates. However, by exploiting repeated observations occurring near the MODIS swath edge, Freeborn et al. (2014a) showed that variations in the exact sub-pixel placement of the fire contribute per-pixel MODIS FRP uncertainties that are normally distributed with σ_η = 26.6%, with simulations demonstrating that at the scale of fire clusters this reduces to less than ~5% for fires containing in excess of ~50 MODIS AF pixels. Such size-dependent FRP uncertainties should be considered during any inter-comparison and/or validation of satellite-based FRP data.

5.2. Fire radiative energy (FRE) estimation

Fire radiative energy (FRE, MJ) is the temporal integral of FRP between two points in time (t_0 and t_n) (Wooster et al., 2005), defined for discrete, evenly spaced, temporal sampling as:

$$FRE = \sum_{t_0}^{t_n} FRP_t \Delta t \tag{6}$$

where FRP is the fire radiative power (MW) at time t and Δt is the time (secs) between FRP retrievals. In fire ecology, the term fire radiative energy [or flux] density (J m^{-2}) is sometimes used (e.g. Kremens et al., 2012; Sparks et al., 2017), but should be limited to situations where estimates of radiant energy release at a point are required.

FRE estimates are best achieved from GEO data, because high imaging frequencies provide the best temporal sampling (Freeborn et al., 2009; Roberts and Wooster, 2008; Li et al., 2018; Ellicott et al., 2009; Roberts et al., 2018a). However, the typically coarser pixel areas of GEO sensors mean they often fail to detect the lower FRP component of a region's fire regime, and a single GEO imager provides neither global coverage nor high-quality observations at very high latitudes (Fig. 4). Numerous methods have attempted to estimate FRE from more infrequent LEO-derived FRP data, for example from the ~ four daily observations provided by MODIS that broadly sample the diurnal fire cycle (e. g. Boschetti and Roy, 2009; Freeborn et al., 2011). The most widely

applied method represents the FRP diurnal cycle using a modified Gaussian (perhaps informed by past GEO-FRP data), tailoring its characteristics via MODIS observations when available (Ellicott et al., 2009; Vermote et al., 2009; Andela et al., 2015; Yin et al., 2019). To counteract effects coming from the relatively small number of daily MODIS observations, and the fact fires are differently detected depending on their position in the MODIS swath which has a 16-day repeat cycle (Freeborn et al., 2009), most LEO-derived FRE estimates are delivered at lower spatio-temporal resolutions (e.g., 0.25°; 8 days).

6. Satellite active fire and FRP products

The number of routinely available GEO and LEO AF products has grown substantially over the last two decades (Table 1), with several LEO products having global and/or multi-decade coverage (Arino et al., 2012; Csiszar et al., 2014; Giglio et al., 2016; Xu et al., 2020). Most use contextual AF detection methods (Section 4.1.3), with the NASA MODIS AF products demonstrating an excellent approach where re-processed Collections are periodically released based on algorithm refinements and updated calibration/geolocation information (Giglio et al., 2003, 2016). Such updates are mostly driven by routine product quality and validation assessments, along with science developments (Justice et al., 2002a, 2002b).

Assessing the absolute accuracy and precision of AF products is difficult for reasons discussed in Section 5. In addition to daytime sunglints, non-burning hot areas and regions of high local thermal contrast can result in AF detection errors of commission in places such as deserts, urban areas, and forest clear cuts (e.g. Schroeder et al., 2008; Kumar and Roy, 2018). Such effects are potentially magnified in higher spatial resolution products (e.g. Schroeder et al., 2014; Zhang et al., 2017). AF

Table 1
LEO and geostationary orbit systems used to generate Active Fire (and for some also FRP) products.

Instrument	Spatial resolution of active fire data	Geographic coverage	Satellite Orbit	Satellite/ Agency
MODIS	1 km	Global	LEO	Terra, Aqua/ NASA
GOES ABI	2 km	75.2° W: North and South America 135° W:Pacific Ocean, Hawaii, North and South America	Geostationary	GOES-E and —W/NOAA
Himawari AHI	2 km	140.7 ° E: East Asia, Australia, Pacific Ocean	Geostationary	Advanced Himawari Imager (AHI), JAXA and JMA
Meteosat SEVIRI	3 km	0°: Europe, Africa, 41.5 E	Geostationary	Eumetsat
VIIRS	375 m, 750 m	Global	LEO	S-NPP, JPSS1/ NOAA 20 NASA/NOAA
NOAA AVHRR	1 km	Global	LEO	POES/NOAA METOP/ Eumetsat
(A)ATSR	1 km	Global (but only nighttime AF product)	LEO	ERS-2[a] and ENVISAT
SLSTR	1 km	Global	LEO	Sentinel-3/ Eumetsat and ESA
HSRS	350 m	Global (but on-demandproducts)	LEO	Firebird Constellation/ DLR

[a] ERS-1 also carried an ATSR sensor, but its MIR channel failed soon after launch.

detection errors of omission are generally related to surface obscuration by cloud (or thick smoke removed incorrectly during cloud masking), fires not burning at the observation time, or small and/or too cool fires having an FRP below the products minimum detection limit (Giglio, 2007; Roy et al., 2008; Roberts et al., 2015; Hall et al., 2019). Commission errors for the best performing products range from a few percent to about 10%, depending on sensor and algorithm specifics. Some of the most mature (e.g., the NASA MODIS products) claim mean global commission errors of around 3% (Giglio et al., 2016). Mature geostationary AF products typically have similar commission errors to LEO products, but higher omission errors due to their larger area pixels and thus higher minimum FRP detection limit (as is apparent in Figs. 5 and 8). Conversely, the higher temporal frequency GEO AF products can sometimes identify fires that are not detected by LEO products, such as those ignited and burned out between LEO overpasses or in cloudy regions where the land surface is viewed briefly by the GEO data as the clouds move (Roberts and Wooster, 2008; Roberts et al., 2015; Hally et al., 2017).

7. AF relationships to fuel consumption and atmospheric variables

7.1. Fuel consumption estimation

One of the earliest applications of satellite data related to landscape fires was toestimate amounts of dry biomass consumed ($M_{consumed}$) (Seiler and Crutzen, 1980). The standard methodology is to combine satellite-derived BA data with biome- and date-dependent fuel consumption per unit area (F_c) estimates, and this is the basis of the widely-used Global Fire Emission Database (GFED, van der Werf et al., 2017). However, the method is unable to operate close to real time since BA data are typically only available after the fire event, and the F_c estimates rely on environmental models driven by meteorological and other data only available with a time delay. As detailed in Section 5 however, FRP measures can provide almost real-time information directly proportional to rates of fuel consumption and smoke emission. FRE (MJ) estimates derived from laboratory-scale 1 Hz FRP measures of mainly cured dry grass fires were shown to be linked to dry biomass consumed via an 'FRE combustion coefficient' (F_c) of 0.37±0.02 kg MJ^{-1} (Wooster et al., 2005):

$$M_{consumed}\ (kg) = 0.37 \times FRE\ (MJ) \tag{7}$$

Confirmation of similar 'combustion coefficient' values for other fuels was subsequently demonstrated in further small-scale fire experiments (e.g. Freeborn et al., 2008; Kremens et al., 2012), and the FRE approach to fuel consumption estimation been applied to landscape-

scale fires using EO data from e.g. Meteosat SEVIRI (Roberts et al., 2005; 2011; 2018a), GOES (Li et al., 2018) and MODIS (Ellicott et al., 2009; Vermote et al., 2009; Kaiser et al., 2012; Andela et al., 2015; Yin et al., 2019; McCarley et al., 2020). However, spaceborne FRP retrievals are subject to perturbations beyond those affecting small-scale field or laboratory studies, potentially altering the effective value of the FRE combustion coefficient. Mota and Wooster (2018) summarize such effects as coming from AF omission errors (Section 4.2), interception of surface-emitted radiation by overlying tree canopies (Roberts et al., 2018b; Mathews et al., 2016; Johnston et al., 2018a, 2018b), atmospheric effects (Wooster et al., 2015), fuel moisture variations (Smith et al., 2013), and potentially fire size-dependent variations in the radiative fraction of the fuel heat yield (Freeborn et al., 2008). Such effects may be responsible for the generally larger and biome-dependent FRE combustion coefficients derived by Kaiser et al. (2012) derived from Global Fire Assimilation System (GFAS)-based FRE estimates and GFED (burned area)-based fuel consumption totals. Despite remaining uncertainties, the FRP and FRE approach provides the only direct route to, respectively, rapidly estimating fuel consumption and smoke emission rates whilst a fire is burning, and the totals of these immediately after a fire has ceased. Further benefits may stem from removing the use of models that are sometimes difficult to parameterize, for example Nguyen and Wooster (2020) demonstrated one of the first EO-based mappings of fuel consumption per unit (F_c) area across Africa, based solely on Meteosat FRE data and 20 m spatial resolution BA mapping.

7.2. Smoke emissions estimation from active fire data

Fire emissions estimation is one of the main applications for EO-derived data on active fires. Johnston et al. (2012) used GFED data and a global atmospheric model to estimate that hundreds of thousands of excess deaths annually are related to exposure to smoke from landscape fires, and Roberts and Wooster (2021) recently revised this estimate upwards based on the FRP-based smoke emissions estimates provided by GFAS. Emissions of a particular smoke species are typically estimated using:

$$M_x = EF_x \times M_{consumed} \tag{8}$$

where M_x is the mass of the emitted species x (g) and EF_x its emission factor (g.kg^{-1}).

However, in part due uncertainties in the 'combustion coefficient' values of Eq. (7) associated with different satellite datasets and/or biomes (see Section 6.1) there is an interest in relating spaceborne FRP estimates directly to rates of smoke emission (R_x), first demonstrated by Ichoku and Kaufman (2005):

(a) (b) (c)
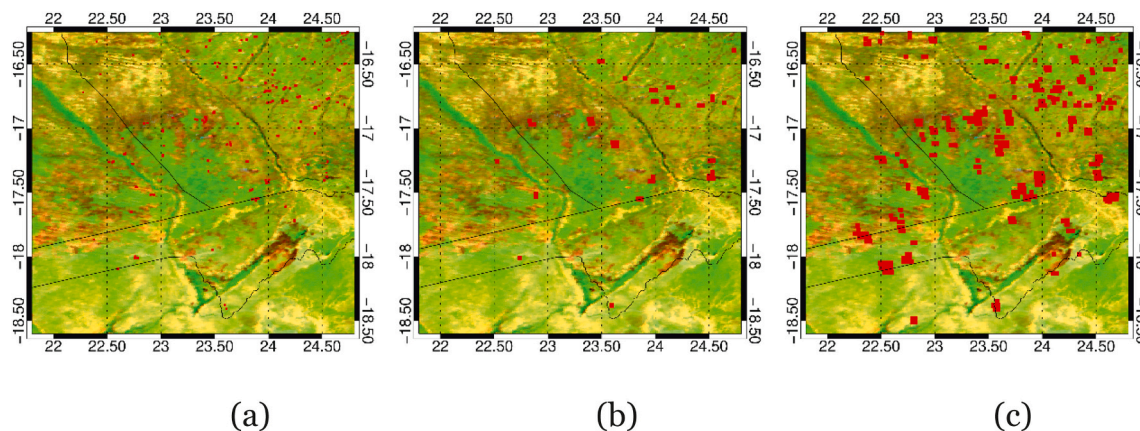
Fig. 8. Active fire detections made on 31st August 2017 (red) in a region of southern Africa using (a) Terra MODIS and Aqua MODIS, (b) Meteosat SEVIRI observations made near-simultaneously with MODIS, and (c) all SEVIRI data collected over that day (24-h). Background is a MODIS surface reflectance image (RGB: 2.1 μm, 0.8 μm and 0.6 μm). (For interpretation of the references to colour in this figure legend, the reader is referred to the web version of this article.)

$$R_x = C_e^x \times FRP \tag{9}$$

where, R_x is the rate of emission of species x (expressed in kg.s^{-1}) and C_e^x is the emission coefficient for species x (kg.MJ^{-1}).

Values of C_e^x are typically derived from comparisons between satellite-derived FRP datasets and the emitted species in question, primarily at present particulate matter (PM) amounts estimated via aerosol optical depth (AOD) measures (Ichoku and Kaufman, 2005; Mota and Wooster, 2018; Nguyen and Wooster, 2020). The approach has been successfully demonstrated for near real-time PM emissions estimation in the U.S. (e.g. Jordan et al., 2008), Canada (e.g. Henderson et al., 2008), and Europe (e.g. Sofiev et al., 2009), and for global-to-continental scale emissions estimation to support science studies (e.g. Vermote et al., 2009; Ichoku and Ellison, 2014; Mota and Wooster, 2018; Nguyen and Wooster, 2020). Table 3 lists the major global fire emissions datasets derived from satellite AF datasets, including GFED since whilst it primarily uses burned area data it uses AF detections to aid BA estimation in certain circumstances (see Section 8).

Fig. 9 shows an emissions inventory intercomparison for seven of the datasets detailed in Table 2 (1–7 July 2016) available globally, both worldwide and for the peak fire month in northern and southern hemisphere Africa. Although it would have been best to show the same smoke aerosol species (in this case, total particulate matter; TPM) for all products, FLAMBE and QFED only provide PM$_{2.5}$ so this is shown instead. Continued uncertainty in fire emissions estimates is evidenced by the more than two times difference among the TPM emissions estimates, and the larger differences when considering PM$_{2.5}$. Other estimates, conducted as yet only for Africa, show similar ranges of estimation (Nguyen and Wooster, 2020). Nevertheless, there appears to be some improvement compared to the factor of 12 difference found even relatively recently (Zhang et al., 2014a, 2014b). Uncertainties stem from a combination of and/or propagation of errors that, depending on the exact method and calculations employed, come from the satellite-derived variables (e.g. AF pixel counts, FRP, and AOD), the aforementioned 'combustion coefficient' conversion factor, the representativeness of the emission factors (EF$_x$), any required smoke injection height and velocity estimates, and the host of applicable model parameterizations/assumptions. Further research is needed to quantify the absolute magnitudes and sources of these uncertainties, and thus improve our current quantification of continental-to-global fire emissions.

8. Relationships to fire regimes and ecosystem variables

AF detections and FRP data are most commonly used to identify fire timing, location, intensity, and smoke emissions source strength. However, they have also been used to infer burned area, fire behavior and fire impacts on the terrestrial environment, both during and after fire events, and to help define areas characterized by different fire regimes.

8.1. Burned area

Satellite data have been used for nearly 40 years to directly map burned area via a fires impact on surface reflectance (Chuvieco et al., 2019). However, in the 1980's and 1990's BA estimates were often calculated using AVHRR-derived AF pixel counts (e.g. Matson et al., 1987) – mainly because AVHRR data are sub-optimal for direct BA mapping (Giglio and Roy, 2020). However, AF errors of omission related to e.g. cloud cover or to fires that were not burning at the satellite observation time mean that AF pixel counts often provide an imperfect proxy for area burned. Fig. 10 shows an area of burned savanna imaged by 30 m Landsat data and overlain with contemporaneous MODIS AF detections. The latter document the spread of the fire but contain extensive spatial gaps, and even interpolation of the AF detections would not fully reconstruct the full BA extent.

Whilst Fig. 10 shows a clear pattern between BA extent and matching AF pixel count, several studies (e.g. Giglio et al., 2013; Hantson et al.,

2013) demonstrate the ratio to be biome-dependent. These include Roy et al. (2008) who found that for low percent tree cover and leaf area index (LAI) landscapes, the MODIS 500 m BA product defined a greater proportion of the landscape as burned than did the MODIS AF product; yet with increasing tree cover (>60%) and LAI (>5) the reverse was often true. Biome-specific calibrations have been undertaken to estimate BA from AF pixel counts (Scholes et al., 1996; Giglio et al., 2013), with for example GFED using nighttime ATSR AF detections (Arino et al., 1999) to estimate BA for the pre-MODIS 1997–2000 period via:

$$BA_{i,t} = \propto_i AF_{i,t}^{\beta_i} \tag{10}$$

where $BA_{i,\,t}$ is the burned area in grid cell i and month t (0.25° grid cells), $AF_{i,\,t}$ is the AF detection for the same cell and time, and $\propto_i$ and β_i are dimensionless and spatially-varying parameters estimated independently using regression of post-2000 ATSR AF pixel counts (Arino et al., 1999) with the 500 m MODIS BA product (Giglio et al., 2013).

Some of the most recent iterations of GFED (e.g. v4.1s; van der Werf et al., 2017) also use satellite AF detections to estimate the additional BA associated with fires too small to be mapped with the MODIS 500 m BA product. Whilst this 'small fire boost' successfully increases BA in many regions, it can also lead to significant errors in locations subject to many AF detection errors of commission (Zhang et al., 2018). This points to the importance of understanding the regional and seasonal dependencies of AF detection errors.

8.2. Rate of spread and intensity and relationships to fire effects

Some of the most ecologically important characteristics of an actively spreading landscape fire are the fire front rate of spread (ROS) and fireline intensity (FLI; Byram, 1959) (Bond and Keeley, 2005). AF data have been related to both – though primarily those based on airborne rather than satellite observations (e.g. Pastor et al., 2006; Paugam et al., 2012). Most satellite AF data use has been limited to mapping wildfire progression across the landscape (e.g. Veraverbeke and Hook, 2013), and whilst ROS estimation has been attempted from LEO (Andela et al., 2019) and occasionally GEO (Liu et al., 2020) AF data, the low spatial and/or temporal resolution of the source data provides limitations. FLI represents the rate of heat release per unit time per unit length of the fire front (kW m^{-1}; Alexander, 1982), and unlike FRP it includes the all heat transfer mechanisms. Thus any FRP-based FLI calculations need to assume a radiant fraction, or simply provide the FLI radiative component only (e.g. Wooster et al., 2004; Riggan et al., 2004; Smith and Wooster, 2005). FRP-derived values of fire heat release may provide links to the effects on plant physiology (Smith et al., 2016), such as pre-and post-fire change in net photosynthesis, tree radial growth, or landscape-scale forest net primary production (NPP) change (e.g. Sparks et al., 2017, 2018; Fig. 11).

8.3. Fire regime characterization

A fire regime describes the prevailing, long-term fire patterns and characteristics of an area, emerging from feedback interactions between climate, vegetation, and the regions natural and anthropogenically driven fires (Whitlock et al., 2010). A fire regimes principle characteristics are fire *frequency, seasonality, spread patterns, intensity* and *fuel consumption* (Bond and Keeley, 2005; Gill, 1975). Satellite AF data have been used to provide contemporary views of landscape fire regimes and to distinguish parameters related to fire size, intensity, severity, and most commonly fire seasonality, frequency and diurnal cycle. Each LEO sensor such as AVHRR, MODIS, and VIIRS typically image areas a few times daily per satellite, enabling fire diurnal cycles to be roughly characterized using either day/night ratios (Giglio et al., 2006; Langaas, 1992) or interpolation between observations (Andela et al., 2015; Ellicott et al., 2009). The TRMM low-inclination, drifting orbit enabled fire diurnal cycles to be characterized from 8-yrs of VIRS data (Giglio, 2007),
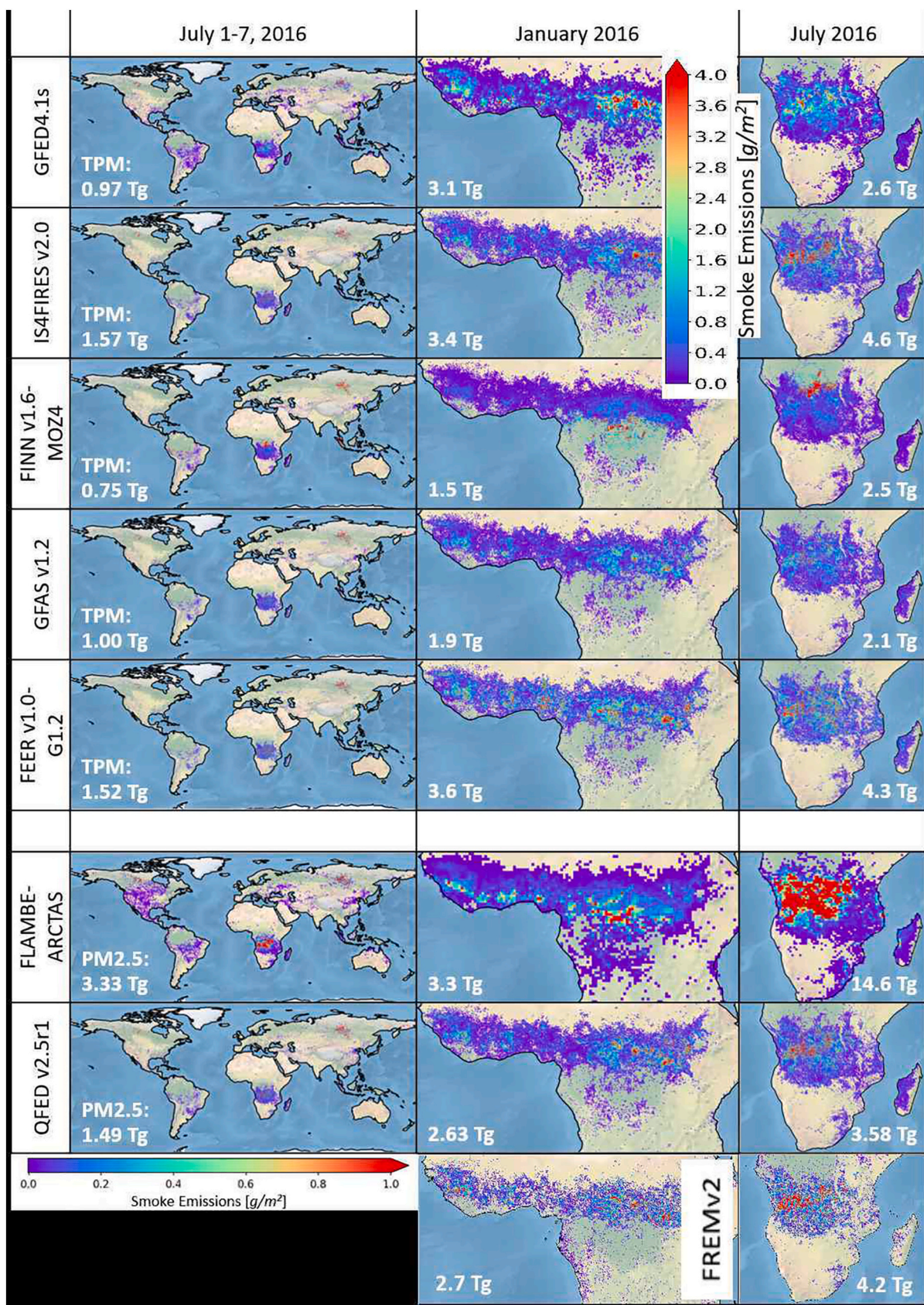
Fig. 9. Landscape fire emissions estimates of total particulate matter (TPM) or particulate matter of 2.5 μm or less aerodynamic diameter (PM$_{2.5}$), as contained within different fire emissions databases (Table 2). Left column: July 1–7, 2016 global distribution; Middle column: January 2016 northern sub-Saharan Africa distribution; Right column: July 2016 southern sub-Saharan Africa distribution. Total emission of the respective smoke species for the respective time periods is indicated on each panel. FREMv2 is based on geostationary data and so is not global.

Table 2

Global fire emissions inventories and real-time monitoring systems based in part on satellite AF data. Note that those not updated in near real time are less appropriate for use in e.g. atmospheric monitoring and forecasting systems. Note that FREMv2 is based on FRP measures derived from GEO systems and so is not global. We focus on here on that derived from Meteosat over Africa.

Emission Dataset Name, version, and access*	Spatial Resolution	Highest Temporal Frequency	Satellite Active Fire Obs Used[#]	Emission Factor/ Coefficient	Data Availability period	Example Reference[@]
FINN_v1.5	1 km	Daily	N_{pix}	EF_x	2002–Present	Wiedinmyer et al., 2011
FLAMBE-ARCTAS	1–4 km	Hourly	N_{pix}	EF_x	2000–Present	Reid et al., 2009
GBBEPx_v2	0.25 deg	Daily	FRP	EF_x	2017–Present	Zhang et al., 2012 Zhang et al., 2017
GFAS_v1.2	0.1 deg	Daily	FRP	EF_x	2001–Present	Kaiser et al., *2012*
GFED_v3.1	0.5 deg	3-hourly	BA, N_{pix}	EF_x	1997–2011	Van der Werf et al., *2010*
GFED_v4.1s	0.25 deg	3-hourly	BA, N_{pix}	EF_x	1995–Present	van der Werf et al., 2017
FEER_v1.0-G1.2	0.1 deg	Daily	FRP	C_e^x	2003–Present	Ichoku and Ellison, 2014
IS4Fires_v2.0	0.1 deg	3-hourly	FRP	C_e^x	2000–Present	Sofiev et al., 2009
QFED_v2.5	0.1 deg	Daily	FRP	C_e^x	2000–Present	Darmenov and Da Silva, *2015*
FREMv2	Per-Pixel & 0.1 deg	15 mins	FRP	C_e^x	2004-Present	Nguyen and Wooster, 2020

*Dataset websites as of March 2021:

FINN (https://www2.acom.ucar.edu/modeling/finn-fire-inventory-ncar);

FLAMBE (not available);

GFAS (https://www.ecmwf.int/en/forecasts/dataset/global-fire-assimilation-system);

GFED (http://www.globalfiredata.org/);

FEER (https://feer.gsfc.nasa.gov/data/emissions/);

IS4Fires (http://is4fires.fmi.fi);

QFED (http://wiki.seas.harvard.edu/geos-chem/index.php/QFED_biomass_burning_emissions);

GBBEP (http://www.ospo.noaa.gov/Products/land/gbbepx/).

[#]This includes the parameter type used in generating the emission dataset (and the sensor/satellite that acquired such observations enclosed in parenthesis): N_{pix}=fire-pixel count; FRP = fire radiative power.

[@]The indicated references are respective representative examples but may not be the most relevant reference for each dataset.
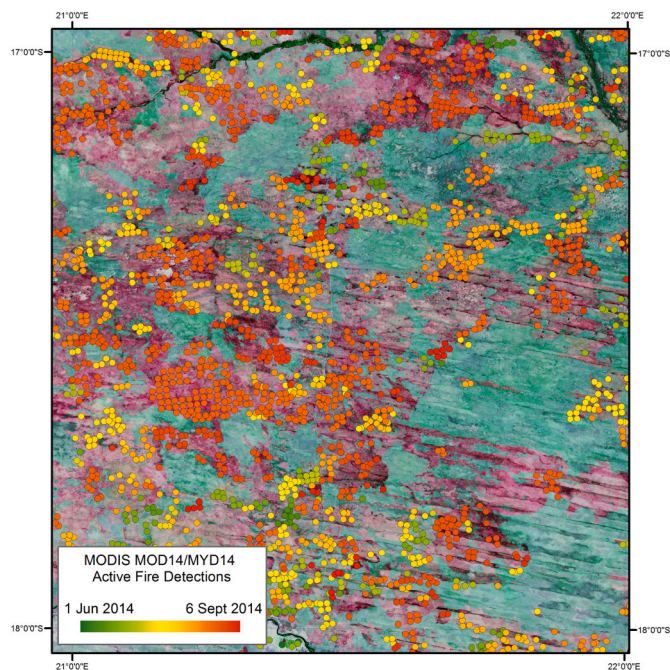

Fig. 10. MODIS 1 km active fire pixel detections (shown with a rainbow colour scale indicating the day of detection over a three month period) superimposed on a Landsat 8 OLI image (R: 2.2 μm, G: 0.86 μm, B: 1.6 μm, burned areas are apparent in magenta tones) acquired on the last day of the MODIS active fire detections (6th September 2014) for 100 km × 100 km over the Caprivi Strip on the border between Angola and Namibia. (For interpretation of the references to colour in this figure legend, the reader is referred to the web version of this article.)

but the high temporal resolution (and constant ground footprint areas) provided by geostationary sensors are optimum for diurnal cycle characterization. GEO data have been applied for this purpose across the Americas (e.g. Prins et al., 1998; Xu et al., 2010; Zhang et al., 2012), east and south-east Asia (e.g. Hyer et al., 2013; Xu et al., 2017) and Africa (e. g. Roberts et al., 2009, 2018a) (Fig. 12).

Satellite AF data indicate that fire diurnal cycles are mostly characterized by mid-afternoon (local solar time) peaks, with less activity (and with generally lower intensities) between late evening and early morning (Giglio, 2007; Hyer et al., 2013; Roberts et al., 2009). During droughts, increased combustion of deep organic soils sometimes results in a less pronounced and/or temporally extended diurnal cycle (e.g. Kaiser et al., 2012; Wooster et al., 2012a, 2018), whereas in agricultural regions a bi-modal diurnal cycle may be driven by local burning practices (Xu et al., 2017). New fire seasons can also sometimes rapidly arise, driven by changes in fire policy and/or enforcement (e.g. Zhang et al., 2020). Further fire regime characteristics derivable from satellite AF data include size distributions, sometimes derived from FRP (e.g. Wooster and Zhang, 2004) though more commonly from BA (e.g. Archibald et al., 2009, 2013). Fire type can sometimes be elucidated, with clusters of adjacent AF pixels deployed to identify spatially contiguous flaming and smoldering areas (Langaas, 1992), and on an instantaneous basis large AF pixel clusters can either be associated with long and narrow fire lines such as found in savannas (e.g. Dwyer et al., 2000), or deep flaming fronts with residual combustion behind, typical of Canadian forest fires (Cahoon et al., 2000). Fire regimes in areas with higher fuel loads and which burn under hotter, drier, and windier conditions generally exhibit higher upper limits of FLI (W.m^{-1}), reaction intensity (W.m^{-2}), and heat release per unit area (J.m^{-2}). These are key fire behavior attributes influencing fires' short- and long-term ecological impact, though thus far their estimation is only rarely attempted from AF data (see Section 7). More commonly, FRE-derived fuel consumption totals (Section 7) have been ratioed against BA data to derive fuel
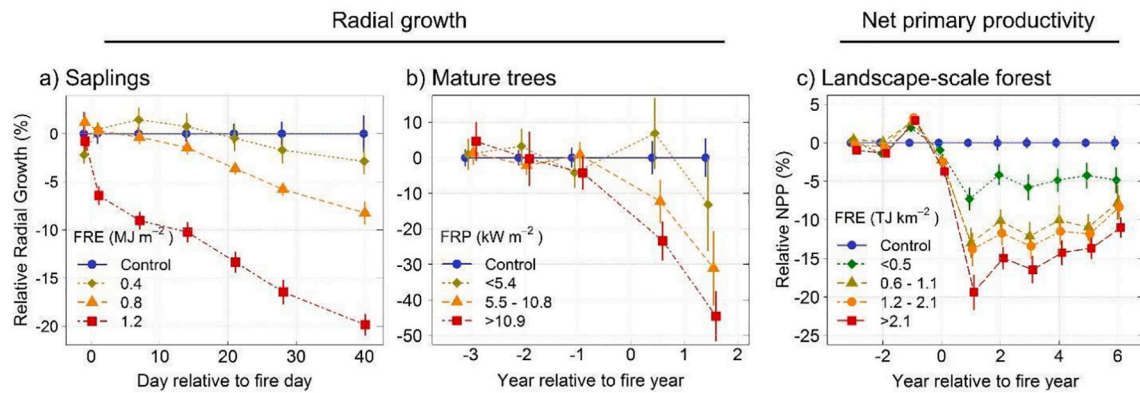
Fig. 11. Radial tree growth and NPP patterns seen across different temporal and spatial scales in areas subject to varying levels of fire activity (as expressed by FRP and FRE per unit area values at (a) 2 yr old *P. contorta* saplings in laboratory experiments and (b) mature (>35 years old) *P. ponderosa* trees burned in stand-scale prescribed fires respectively. Similar patterns were observed in (c) at the regional scale using net FRE per unit area and NPP measures derived from MODIS. See Smith et al. (2017); Sparks et al. (2017; 2018).
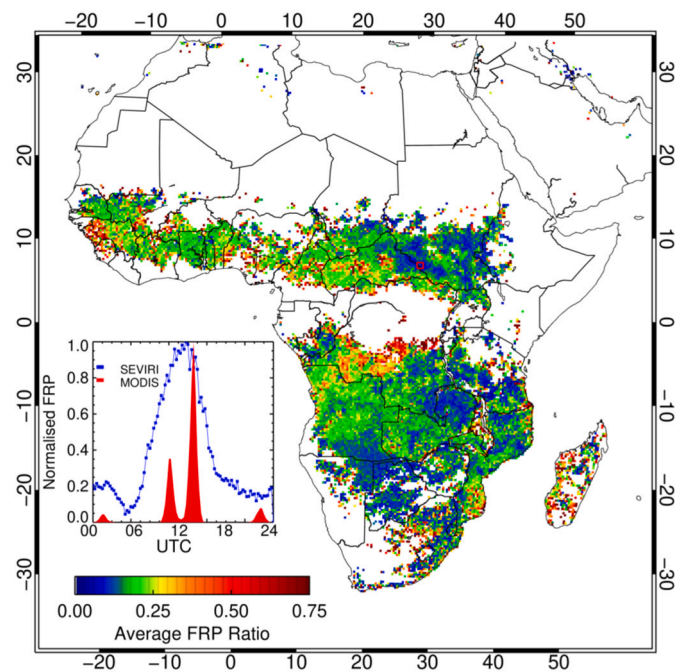
Fig. 12. Fire radiative power (FRP) diurnal cycle variability across Africa, as derived from a year of the 96 daily FRP datasets provided by the geostationary Meteosat FRP-PIXEL product available from the EUMETSAT LSA-SAF (Wooster et al., 2015; Roberts et al., 2015). Generally, the fire diurnal cycle is semi-Gaussian, with a day-time peak and nighttime minima (see inset that shows normalized FRP values from SEVIRI and MODIS), but the timing of the peak spatially varies. The metric shown is the ratio between the summed FRP measured by SEVIRI at only the times of MODIS overpasses, and that measured over the full 24-h cycle. Changes in the timing of the diurnal cycle peak are reflected in changes to this ratio.

consumption per unit area measures (e.g. Roberts et al., 2011; Mota and Wooster, 2018; Nguyen and Wooster, 2020), and have been used to help discriminate identical fire regimes happening at different times of the year under variable meteorological conditions (e.g., Andela et al., 2015; Boschetti and Roy, 2009; Freeborn et al., 2016). FRP distributions themselves have revealed regional as well as intra-biome fire regime variations (Wooster and Zhang, 2004; Ichoku et al., 2008; Giglio et al., 2006; Laurent et al., 2019), though such differences may be due to variations in an unknown combination of fire behavior attributes (e.g. radiant fraction, sub-pixel active fire area, fire intensity) coupled with

influences such as canopy overstory effects (Roberts et al., 2018b).

AF products are particularly well suited for characterizing fire seasons, or the times of the year when large and intense fires are most prevalent. A variety of temporal metrics (e.g., start and end dates, peak month, and fire season duration etc.) have been derived from both AF pixel counts and FRP data, and used to map regional to global variations in fire seasonality (e.g. Dwyer et al., 2000; Giglio et al., 2006). Locations where the fire season leads or lags seasonal weather may indicate the degree of control that humans exert on a regions fire regime (Le Page et al., 2010). For example, across much of northern Africa, rural communities purposely ignite early season fires under mild weather conditions to create a patchwork of fuel breaks in an attempt to limit the uncontrolled spread of more intense and more ecologically damaging late season fires (Laris, 2002). Agricultural residue burning periods similarly closely coincide with the timing of crop-specific planting and harvesting (Korontzi et al., 2006; McCarty et al., 2009; Zhang et al., 2018, 2020).

Accumulating many years of AF observations allows retrieval of long-term attributes, such as fire return interval (average number of years between successive fires), fire frequency (the inverse of fire return interval), and measures of interannual fire variability and trend. However, derived chronologies of annual fire occurrence have been more commonly extracted from BA time-series (Devineau et al., 2010; Freeborn et al., 2014c). Instead, the simplest and most common AF analog has probably been the count of AF pixels detected per unit time and per unit area, referred to as both fire frequency and fire density (Chuvieco et al., 2008; Csiszar et al., 2005; Di Bella et al., 2006; Soja et al., 2004). Temporal trends in AF pixel counts are most often used to infer changes in fire occurrence and when associated with time-series of climate, land cover, and anthropogenic variables have been used to identify locations of shifting fire regimes potentially associated with anthropogenic or climatic trends (Aragao and Shimabukuro, 2010; Arino et al., 2012; Gregoire and Simonetti, 2010; Pricope and Binford, 2012).

9. Online AF data delivery and mapping systems

Whilst certain of the AF products outlined in Section 6 have been available for several decades, widespread product delivery in easily accessible formats has been available for only around half this time. The MODIS Rapid Response System was the first attempt to provide near real-time global AF data (Justice et al., 2002a), subsequently evolving into the NASA Fire Information for Resource Management System (FIRMS) (Davies et al., 2014). These developments are part of a growing trend of "analysis ready data" (ARD), which aims to reduce the EO data pre-processing burden on users and enable easier and more immediate analyses. AF data are made available typically with very low data

latency rates via these and other systems, generally within a few hours or less of the observation time.

AF detections have been available in analysis ready form for more than two decades, and this has helped spread their use in multiple applications. Many of these need not expose the user to detailed knowledge of the methods and algorithms (outlined in earlier Sections) that have been used to produce the AF data. Applications include strategic land and fire management, no-burning compliance monitoring, wildlife conservation, detection of illegal logging and/or poaching within protected areas, monitoring air pollution and improved understanding of fire regimes. As applications for AF data have evolved and matured, users have further articulated their information requirements (e.g., Trigg and Roy, 2007; Mouillot et al., 2014; Davies et al., 2014), which in turn has led to more customized data products, more functional and accessible online data mapping and delivery systems including a wider variety of variables, and most recently also mobile accessible applications. Whilst some users simply wish to visualize AF data on a map, and others want to download it for their own analyses, increasingly there is a move to also provide broader contextual information in a single online application (e.g. land cover; atmospheric composition; fire risk, BA).

AF fire data delivery systems can be classified into three groups: 1) direct providers, who process and distribute their own AF data; 2) brokers, who take AF data from a direct provider and add value by customizing the information to serve specific user communities; and 3) those that are both direct providers and brokers. The latter often process data collected 'locally' in real-time via a so-called satellite direct reception (DR) or direct broadcast (DB) station, but also acquire additional AF data from others to provide broader geographic coverage. AF data users are now faced with a huge choice of data portals, and Appendix 2 provides detail on four key examples currently operating. We also include therein an example of how such data are used, in this case in support of national park fire management. Users select their most appropriate information delivery system based on data type and coverage, latency (time from satellite overpass to user availability), ease of use, and how the AF data can be viewed and queried alongside other types of information. GEO or DR-based LEO data feeds generally have some of the lowest data latency times, but more recently even non-DR equipped data portals for MODIS and VIIRS AF data, such as NASA FIRMS (part of NASA's Land, Atmosphere Near real-time Capability for EOS (LANCE)) offer AF data updates usually within 2.5 h of the observation time, though some specifics of the near real-time (NRT) AF products served may differ from those of the "standard" data products. New data feeds are following this trend, with AF detections and FRP data Sentinel-3 (Wooster et al., 2012b; Xu et al., 2020) produced in two versions, NRT within a few hours of data capture (https://metis.eumetsat.int/frp/), and non-time critical (NTC) a few days later .

10. Future priorities in active fire remote sensing

10.1. Dataset priorities

NRT and higher spatial and temporal resolution satellite AF and FRP products are a priority for the applications and science communities. Errors of AF commission and in particular omission should continue to be reduced, through sensor and algorithm development, robust validation, and provision of improved ancillary datasets such as masks optimized for the AF-application, e.g. cloud masks which do not mask out smoke contaminated areas, appropriate land/water maps, and maps of static IR emitters (e.g. gas flares/volcanoes and potentially persistent false alarms due to e.g. specific industry or building types). Such developments are required to meet the temporal (1–6 h) and spatial (0.25–3 km) resolution and FRP retrieval uncertainty (10% integrated over a pixel) target specifications outlined by the Global Climate Observing System (GCOS) Essential Climate Variable (ECV) programme (GCOS, 2016) and proposed by GOFC/GOLD and the Committee on EO Satellites (CEOS) Land Product Validation (LPV) working groups

(Boschetti et al., 2009). The need for long-term, climate quality, AF products offering global coverage remains paramount, and this entails systematic product generation, quality control, algorithm maintenance and when necessary reprocessing. Without reprocessing using updated calibration and geolocation information, and improved algorithms refined in response to routine product quality assessment periodic validations (Section 6), AF products become less suitable for addressing climate science questions.

In addition to improving AF detection algorithms, efforts should focus on developing AF products maximizing use of currently available data, such as through blending GEO and LEO observations (e.g. Zhang et al., 2020). A long-standing GOFC/GOLD goal is the development of a global geostationary AF system, which is increasingly relevant given the improved AF fire detection apability of the new generation of GEO satellites. AF detection and FRP data have recently become available in NRT from Meteosat, Meteosat Indian Ocean, Himawari and GOES-E and —W using the same FTA algorithm originally developed for Meteosat SEVIRI (Roberts and Wooster, 2008; Wooster et al., 2015; Xu et al., 2017, 2021a). Similarly, the availability of Landsat and Sentinel-2 imagery having pixel sizes in the tens of meters provides detailed SWIR-based AF detection that may complement coarser spatial resolution but more frequently available AF products, if only initially for validation of the latter. The increasing number of very high spatial resolution (1–3 m) sensors should also be evaluated for their potential use in AF detection. Development of additional ancillary datasets, such as those related to fuel load per unit area, and biome, season and fuel-moisture dependent trace gas and aerosol emissions factors (EFs), is required to further improve fire emissions estimation.

10.2. EO sensor and mission priorities

This review has reiterated that to provide optimum data for AF remote sensing, a typical sensor requires co-registered channels in the MIR (3–5 μm) and LWIR (8–14 μm), a co-located VIS or NIR channel to aid daytime masking of false alarms and cloud. The exact spectral placement of each channel is less prescriptive, but for example the 3.959 μm "fire channel" of MODIS was selected due to its relative insensitivity to atmospheric water vapor absorption and avoidance of the CO_2 absorption window beyond ~4 μm (Kaufman et al., 1998). Of key importance for FRP retrieval are MIR measurements across a sufficient dynamic range to provide good quality, unsaturated data over the highest intensity and/or largest fires, as well as over the ambient temperature background. Without the former, the FRP of the most strongly emitting fires cannot be gauged, and without the latter the AF pixels themselves may not even be reliably detected. The required upper end of the MIR channel dynamic range needs to be set according to the sensors ground pixel footprint area, since the same fire will form a greater proportion of a smaller rather than larger pixel (MODIS 1 km^2 pixels have ~500 K saturation temperature vs. ABI 4 km^2 pixels have ~400 K). For the 60 m spatial resolution MIR band of the proposed Hyperspectral Infrared Imager (HyspIRI) payload, Realmuto et al. (2015) specified a 1200 K saturation temperature. As with MODIS and SLSTR, such wide dynamic ranges sometimes require two MIR detectors, or one detector operating with dual integration times or gain settings (e.g. BIRD HSRS and VIIRS). Other beneficial sensor attributes include limiting pixel area growth across the swath (as done with VIIRS and SLSTR; Schroeder et al., 2014; Xu et al., 2021b), a SWIR channel operating at night to aid hotspot detection, discrimination of fires from higher temperature targets such as gas-flares, and FRP estimation from the latter (Fisher and Wooster, 2018, 2019). SWIR wavebands centered around 2.2 μm appear most effective, and night-time use of a broad day-night (low light level) band (0.5–0.9 μm) similar to that of VIIRS can also be considered. SWIR-based AF detection is also possible by day if ground pixel footprints are small enough.

High temporal resolution AF data is required for operational fire monitoring, warning and fire-fighting applications, and to provide the

most reliable estimation of FRE via FRP temporal integration. GEO systems meet this goal, with the newest such as Himawari (Bessho et al., 2016; Xu et al., 2017), Meteosat Second Generation (soon to be super-seded by Meteosat Third Generation [MTG]; Roberts and Wooster, 2008), GEO-KOMPSAT-2A and Feng-Yun 4A (Yang et al., 2017), and GOES-R (Schmit et al., 2017; Xu et al., 2017; 2021) including MIR bands having suitably extended dynamic ranges, and offering full-disk temporal resolutions as high as 10 min. However, their larger pixel areas result in minimum FRP detection limits typically at least 4× higher than from the nadir views of LEO sensors – so they generally cannot detect a substantial number of fires that MODIS type sensors would identify if they viewed the same location at the same time. MTG will offer 1 km data every 2.5 min over some areas, a first for the AF application, and even in densely populated Europe this may provide sufficient capability to usefully detect a significant number of newly ignited fires in advance of public call ins. Use of highly elliptical orbits could be explored to provide a high latitude, high temporal resolution AF capability. An achievable future GEO goal that would cover many of the applications supported by current LEO systems would be 500 m spatial resolution geostationary-based AF detection, and the Chinese Meteorological Agency (CMA) GF4 GEO satellite already includes a 400 m MIR channel that demonstrates this is possible (Lu et al., 2020).

An option to provide high spatial detail, low commission error AF data at increased temporal resolutions is via constellations of LEO systems placed to cover different overpass times. LEO capabilities continue to improve, and compared to MODIS Sentinel-3 SLSTR offers a some-what improved AF detection sensitivity due to its on average smaller pixel footprint area (Xu et al., 2020; 2021; Fig. 3), whilst VIIRS' 375 m data offers a sensitivity around 10× better (Schroeder et al., 2014; Zhang et al., 2017). Going beyond the spatial resolution of VIIRS may provide diminishing returns, since the latter can already identify active areas of combustion of <20 m^2, and over some landscapes high AF errors of commission can result from the IR clutter present in very finely detailed thermal imagery (Schroeder et al., 2014; Zhang et al., 2017). Performance trade-offs between the existing style of often larger satellites using cooled sensor technology and lower cost smaller missions that might enable lower-cost constellation development, possibly using un-cooled detectors if their performance can be demonstrated (e.g. Wild-FireSat; Johnston et al., 2020), should be examined.

10.3. Other research priorities

Beyond datasets and sensors, there remain several primacies for ongoing research in AF remote sensing. These include a better under-standing of errors and uncertainties in AF detection, FRP retrieval and fire emissions estimation, both spatially (e.g. by biome), temporally (e.g. diurnally, seasonally) and with respect to different sensors, products and observational (e.g. atmospheric and view angle) effects. Validation of AF products remains challenging, due to the ephemeral and dynamic nature of fire and to difficulties in obtaining co-located simultaneous and in-dependent reference observations. On a global scale this has been limited to joint use of ASTER and Terra MODIS (see Section 1), and with Terra nearing its end of life there is a need to develop a validation strategy covering a wider array of instruments and times of day. Simi-larly, a uniform protocol to validate spaceborne FRP retrievals is required, particularly as it is a designated GCOS ECV and one which is still at the lowest validation stage according to the CEOS LPV validation hierarchy. Understanding the lower FRP components of a regions fire regime and how this is included or excluded by different AF data products remains important, as are ways to adjust for this when neces-sary. The ability to map fireline rates of spread remains a goal for many fire management applications, as is the need to further promote assim-ilation of NRT AF data into time-coupled weather-fire behavior model-ling frameworks (Coen and Schroeder, 2013). Research on the conversion between FRP, FRE and fuel consumption, trace gas and aerosol emissions continues to be a priority, as does the reconciling of

such estimates with those from alternative (e.g. burned area) based approaches. Finally, the accuracy and usefulness of EO methods for flaming/smoldering fire discrimination - including via use of phenom-ena such as detection of landscape fire potassium emission lines - needs to be further examined, as does the need and ability to optimize any applied emissions factors used in subsequent smoke emissions calculations.

11. Summary and conclusion

Observing landscape fires from space has a strong heritage, stretch-ing back to the 1980's with NOAA AVHRR. Since then, satellite active fire (AF) data have become very widely used by scientists and govern-ment agencies, and the number of spaceborne sensors equipped with measurement capabilities relevant to the AF application, including with 'fire-optimized' thermal channel dynamic ranges, has greatly increased. The NASA MODIS AF product suite is the most widely utilized, and the ease of access to these and other AF data through numerous data portals has proliferated beyond science to allow routine monitoring and reporting - as evidenced by their deployment by the media during the recent [2019] Amazonian fire activity increase (Kelley et al., 2021) and during the 2019/2020 Australian black Summer bushfires (Abram et al., 2021). Although these recent events have highlighted the relevance and importance of satellite AF products (e.g. Escobar, 2019), they have also reinforced the need for the community of data producers to more clearly communicate the limitations as well as benefits of each AF product, so as to reduce interpretation inaccuracies.

AF products have evolved from reporting the timing and location of actively burning fires to now include measures such as fire effective temperature, area and fire radiative power (FRP). Near real-time (NRT) EO data streams have allowed the FRP method to be used to deliver smoke emissions source strength information to a variety of atmospheric modelling systems, for example in support air quality forecasting. Future satellite missions, including higher spatial resolution GEO systems and increased numbers of AF-capable LEO systems, including the future possibly of small-satellite constellations, provide further opportunities for advancing both science and operational applications as their per-formance evolves. A key constraint remains the scarcity of reference data suitable for validating contemporaneous AF detections and FRP retrievals. Communities such as GOFC/GOLD and CEOS LPV are encouraged to continue to lobby space agencies to develop and launch missions that include sensors whose characteristics are optimized for the AF application, and often only relatively small adjustments to the initially planned characteristics are required – as was the case for example with Sentinel-3 SLSTR and Meteosat Third Generation. Looking forward, continuing climate and environmental change may potentially shift certain drivers of landscape fire (Rogers et al., 2020). Apparent policy or policy enforcement shifts appear able to rapidly alter fire characteristics over large regions (Sembhi et al., 2020), and the health impacts of the poor air quality that can come with landscape burning is a growing concern. We can therefore expect the relevance and importance of satellite AF remote sensing to continue to grow.

Declaration of Competing Interest

The authors declare that they have no known competing financial interests or personal relationships that could have appeared to influence the work reported in this paper.

Acknowledgments

award DMS-1520873, and C.I. is also grateful for partial support received from the NOAA Educational Partnership Program under Agreement No. #NA16SEC4810006. The National Aeronautics and Space Administration supported A.M.S. under award LCLUC-80NSSC20K1488. This review is an official output from the Global Observation of Forest Cover/Global Observation of Landcover Dynamics (GOFC/GOLD) Fire Programme (https://gofcgold.org/).

Appendix A. Supplementary data

Supplementary data to this article can be found online at https://doi.org/10.1016/j.rse.2021.112694.

References

Abram, N.J., Henley, B.J., Gupta, A.S., Lippmann, T.J., Clarke, H., Dowdy, A.J., Sharples, J.J., Nolan, R.H., Zhang, T., Wooster, M.J., Wurtzel, J.B., 2021. Connections of climate change and variability to large and extreme forest fires in Southeast Australia. Commun. Earth Environ. 2 (1), 1–17.

Àgueda, A., Pastor, E., Pérez, Y., Planas, E., 2010. Experimental study of the emissivity of flames resulting from the combustion of forest fuels. Int. J. Therm. Sci. 49 (3), 543–554.

Ahern, F., Goldammer, G., Justice, C.O. (Eds.), 2001. Global and Regional Vegetation Fire Monitoring From Space: Planning a Coordinated International Effort. SPB Academic Publishing, The Hague, The Netherlands. ISBN 90-5103-140-8.

Alexander, M.E., 1982. Fire behavior in aspen slash fuels as related to the Canadian Fire Weather Index. Can. J. For. Res. 12 (4), 1028–1029.

Amici, S., Wooster, M.J., Piscini, A., 2011. Multi-resolution spectral analysis of wildfire potassium emission signatures using laboratory, airborne and spaceborne remote sensing. Remote Sens. Environ. 115 (8), 1811–1823.

Amraoui, M., DaCamara, C.C., Pereira, J.M.C., 2010. Detection and monitoring of African vegetation fires using MSG-SEVIRI imagery. Remote Sens. Environ. 114 (5), 1038–1052.

Andela, N., Kaiser, J.W., van der Werf, G.R., Wooster, M.J., 2015. New fire diurnal cycle characterizations to improve fire radiative energy assessments made from MODIS observations. Atmos. Chem. Phys. 15, 8831–8846.

Andela, N., Morton, D.C., Giglio, L., Paugam, R., Chen, Y., Hantson, S., Werf, G.R., Randerson, J.T., 2019. The global fire atlas of individual fire size, duration, speed and direction. Earth Syst. Sci. Data 11 (2), 529–552.

Aragao, L.E.O.C., Shimabukuro, Y.E., 2010. The incidence of fire in Amazonian forests with implications for REDD. Science. 328, 1275–1278.

Archibald, S., Roy, D.P., van Wilgen, B.W., Scholes, R.J., 2009. What limits fire? An examination of drivers of burnt area in Southern Africa. Glob. Chang. Biol. 15, 613–630.

Archibald, S., Lehmann, C.E., Gómez-Dans, J.L., Bradstock, R.A., 2013. Defining pyromes and global syndromes of fire regimes. Proceed. Nation. Acad. Sci. 110, 6442–6447.

Arino, O., Rosaz, J.-M., Goloub, P., 1999. The ATSR world fire atlas: a synergy with "Polder" aerosol products. Earth Observ. Quart. 64 (8).

Arino, O., Casadio, S., Serpe, D., 2012. Global night-time fire season timing and fire count trends using the ATSR instrument series. Remote Sens. Environ. 116, 226–238.

Atwood, E.C., Englhart, S., Lorenz, E., Halle, W., Wiedemann, W., Siegert, F., 2016. Detection and characterization of low temperature peat fires during the 2015 fire catastrophe in Indonesia using a new high-sensitivity fire monitoring satellite sensor (FireBird). PLoS One 11 (8).

Bessho, K., Date, K., Hayashi, M., Ikeda, A., Imai, T., Inoue, H., Kumagai, Y., Miyakawa, T., Murata, H., Ohno, T., Okuyama, A., 2016. An introduction to Himawari-8/9—Japan's new-generation geostationary meteorological satellites. J. Meteorol. Soc. Japan. Ser. II 94 (2), 151–183.

Bond, W.J., Keeley, J.E., 2005. Fire as a global 'herbivore': the ecology and evolution of flammable ecosystems. Trends Ecol. Evol. 20, 387–394. https://doi.org/10.1016/j.tree.2005.04.025.

Boschetti, L., Roy, D.P., 2009. Strategies for the fusion of satellite fire radiative power with burned area data for fire radiative energy derivation. J. Geophys. Res.-Atmos. 114 https://doi.org/10.1029/2008JD011645. D20302.

Boschetti, L., Roy, D.P., Justice, C.O., 2009. International Global Burned Area Satellite Product Validation Protocol Part I–Production and Standardization of Validation Reference Data. Committee on Earth Observation Satellites, Maryland, MD, USA, pp. 1–11.

Bowman, D.M., Balch, J.K., Artaxo, P., Bond, W.J., Carlson, J.M., Cochrane, M.A., D'Antonio, C.M., DeFries, R.S., Doyle, J.C., Harrison, S.P., Johnston, F.H., 2009. Fire in the earth system. Science 324 (5926), 481–484.

Briess, K., Jahn, H., Lorenz, E., Oertel, D., Skrbek, W., Zhukov, B., 2003. Fire recognition potential of the bi-spectral infrared detection (BIRD) satellite. Int. J. Remote Sens. 24 (4), 865–872.

Brönnimann, S., Volken, E., Lehmann, K., Wooster, M., 2009. Biomass burning aerosols and climate. A 19th century perspective. Meteorologische Zeitschrift (Berlin) 18.

Byram, G.M., 1959. Combustion of forest fuels. In: Davis, K.P. (Ed.), Forest Fire: Control and Use. McGrawHill, New York, pp. 90–123.

Cahoon Jr., D.R., Stocks, B.J., Levine, J.S., Cofer III, W.R., O'Neill, K.P., 1992. Seasonal distribution of African savanna fires. Nature 359 (6398), 812.

Cahoon, D.R., Stocks, B.J., Alexander, M.E., Baum, B.A., Goldammer, J.G., 2000. Wildland fire detection from space: Theory and application. In: Innes, J.L.,

Beniston, M., Verstraete, M.M. (Eds.), Biomass Burning and its Inter-Relationships with the Climate System. Springer Netherlands, Dordrecht, pp. 151–169.

Cheney, P., Sullivan, A. (Eds.), 2008. Grassfires: Fuel, Weather and Fire Behaviour. Csiro Publishing.

Chuvieco, E., Giglio, L., Justice, C., 2008. Global characterization of fire activity: toward defining fire regimes from earth observation data. Glob. Chang. Biol. 1488–1502.

Chuvieco, E., Mouillot, F., van der Werf, G.R., San Miguel, J., Tanasse, M., Koutsias, N., García, M., Yebra, M., Padilla, M., Gitas, I., Heil, A., 2019. Historical background and current developments for mapping burned area from satellite earth observation. Remote Sens. Environ. 225, 45–64.

Coen, J.L., Schroeder, W., 2013. Use of spatially refined satellite remote sensing fire detection data to initialize and evaluate coupled weather-wildfire growth model simulations. Geophys. Res. Lett. 40, 5536–5541.

Coheur, P.-F., Clarisse, L., Turquety, S., Hurtmans, D., Clerbaux, C., 2009. IASI measurements of reactive trace species in biomass burning plumes. Atmos. Chem. Phys. 9 (15), 5655–5667.

Csiszar, I., Sullivan, J., 2002. Recalculated pre-launch saturation temperatures of the AVHRR 3.7 μm sensors on board the TIROS-N to NOAA-14 satellites. Int. J. Remote Sens. 23 (24), 5271–5276.

Csiszar, I., Abuelgasim, A., Li, Z., Jin, J., Fraser, R., Hao, W.-M., 2003. Interannual changes in active fire detectability in North America from long-term records of the advanced very high resolution radiometer. J. Geophys. Res. 108 (D2), 4075.

Csiszar, I., Denis, L., Giglio, L., Justice, C., Hewson, J., 2005. Global fire activity from two years of MODIS data. Int. J. Wildland Fire 117–130.

Csiszar, I.A., Justice, C.O., Goldammer, J.G., Lynham, T., de Groot, W.J., Prins, E.M., Elvidge, C.D., Oertel, D., Lorenz, E., Bobbe, T., Quayle, B., Davies, D., Roy, D., Boschetti, L., Korontzi, S., Ambrose, S., Stephens, G., 2013. The GOFC/GOLD fire mapping and monitoring theme: Assessment and strategic plans. In: Qu, J.J., Sommers, W., Yang, R., Riebau, A., Kafatos, M. (Eds.), Remote Sensing Modeling and Applications to Wildland Fires, 2013. Springer-Verlag, co-published with Tsinghua University Press, 550 pp. ISBN 978-3-642-32529-8.

Csiszar, I., Schroeder, W., Giglio, L., Ellicott, E., Vadrevu, K.P., Justice, C.O., Wind, B., 2014. Active fires from the Sumi NPP visible infrared imaging radiometer suite: product status and first evaluation results. J. Geophys. Res.-Atmos. 119. https://doi.org/10.1002/2013JD020453.

Darmenov, A., Da Silva, A., 2015. The quick fire emissions dataset (QFED)–documentation of versions 2.1, 2.2 and 2.4. In: NASA Technical Report Series on Global Modeling and Data Assimilation, NASA TM-2015-104606, p. 38.

Davies, D.K., Murphy, K.J., Michael, K., Becker-Reshef, I., Justice, C.O., Boller, R., Braun, S., Schmaltz, J., Wong, M., Pasch, A., Dye, T., da Silva, A., Goodman, M., Morin, P., 2014. The use of NASA LANCE imagery and data for near-real-time application. In: Lippitt, C., Stow, D., Coulter, L. (Eds.), Time Sensitive Remote Sensing. Springer Press, pp. 165–182.

Dennison, P.E., Charoensiri, K., Roberts, D.A., Peterson, S.H., Green, R.O., 2006. Wildfire temperature and land cover modeling using hyperspectral data. Remote Sens. Environ. 100 (2), 212–222.

Devineau, J.L., Fournier, A., Nignan, S., 2010. Savanna fire regimes assessment with MODIS fire data: their relationship to land cover and plant species distribution in western Burkina Faso (West Africa). J. Arid Environ. 74, 1092–1101.

Di Bella, C.M., Jobbagy, E.G., Paruelo, J.M., Pinnock, S., 2006. Continental fire density patterns in South America. Glob. Ecol. Biogeogr. 15, 192–199.

Di Biase, V., Laneve, G., 2018. Geostationary sensor based forest fire detection and monitoring: an improved version of the SFIDE algorithm. Remote Sens. 10 (5), 741.

Dozier, J., 1981. A method for satellite identification of surface temperature fields of subpixel resolution. Remote Sens. Environ. 11, 221–229.

Duff, T.J., Penman, T.D., 2021. Determining the likelihood of asset destruction during wildfires: modelling house destruction with fire simulator outputs and local-scale landscape properties. Saf. Sci. 139, 105196.

Dwyer, E., Pinnock, S., Gregoire, J.M., Pereira, J.M.C., 2000. Global spatial and temporal distribution of vegetation fire as determined from satellite observations. Int. J. Remote Sens. 21, 1289–1302.

Eidenshink, J.C., Faundeen, J.L., 1994. The 1 km AVHRR global land data set: first stages in implementation. Int. J. Remote Sens. 15 (17), 3443–3462.

Ellicott, E., Vermote, E., Giglio, L., Roberts, G., 2009. Estimating biomass consumed from fire using MODIS FRE. Geophys. Res. Lett. 36, 13. https://doi.org/10.1029/2009GL038581.

Ellyett, C.D., Fleming, A.W., 1974. Thermal infrared imagery of the burning mountain coal fire. Remote Sens. Environ. 3 (1), 79–86.

Elvidge, C.D., Kroehl, H.W., Kihn, E.A., Baugh, K.E., Davis, E.R., Hao, W.M., 1996. Algorithm for the retrieval of fire pixels from DMSP operational linescan system data. In: Levine, J.S. (Ed.), Biomass Burning and Global Change: Remote Sensing, Modeling and Inventory Development, and Biomass Burning in Africa, vol. 1. MIT Press, Cambridge, pp. 73–85.

Elvidge, C.D., Zhizhin, M., Hsu, F.-C., Baugh, K.E., 2013. VIIRS nightfire: satellite pyrometry at night. Remote Sens. 5, 4423–4449. https://doi.org/10.3390/rs5094423.

Elvidge, C.D., Zhizhin, M., Hsu, F.-C., Baugh, K., Khomarudin, M.R., Vetrita, Y., Sofan, P., Suwarsono, and Hilman, D., 2015. Long-wave infrared identification of moldering peat fires in Indonesia with nighttime Landsat data. Environ. Res. Lett. https://doi.org/10.1088/1748-9326/10/6/065002, 10.065002.

Escobar, H., 2019. Amazon fires clearly linked to deforestation, scientists say. Science 6456, 853.

Filizzola, C., Corrado, R., Marchese, F., Mazzeo, G., Paciello, R., Pergola, N., Tramutoli, V., 2017. RST-FIRES, an exportable algorithm for early-fire detection and monitoring: description, implementation, and field validation in the case of the MSG-SEVIRI sensor. Remote Sens. Environ. 192, e2–e25.

Fisher, D., Wooster, M., 2018. Shortwave IR adaption of the mid-infrared radiance method of fire radiative power (FRP) retrieval for assessing industrial gas flaring output. Remote Sens. 10 (2), 305.

Fisher, D., Wooster, M.J., 2019. Multi-decade global gas flaring change inventoried using the ATSR-1, ATSR-2, AATSR and SLSTR data records. Remote Sens. Environ. 232, 111298.

Fisher, D., Wooster, M.J., Xu, W., Thomas, G., Lestari, P., 2020. Top-down estimation of particulate matter emissions from extreme tropical peatland fires using geostationary satellite fire radiative power observations. Sensors 20 (24), 7075.

Flannigan, M.D., Vonder Haar, T.H., 1986. Forest fire monitoring using the NOAA satellite AVHRR. Can. J. For. Res. 16 (5), 975–982.

Flasse, S.P., Ceccato, P., 1996. A contextual algorithm for AVHRR fire detection. Int. J. Remote Sens. 17, 419–424.

Freeborn, P.H., Wooster, M.J., Hao, W.M., Ryan, C.A., Nordgren, B.L., Baker, S.P., Ichoku, C., 2008. Relationships between energy release, fuel mass loss, and trace gas and aerosol emissions during laboratory biomass fires. J. Geophys. Res.-Atmos. 113 (D1).

Freeborn, P.H., Wooster, M.J., Roberts, G., Malamud, B.D., Xu, W., 2009. Development of a virtual active fire product for Africa through a synthesis of geostationary and polar orbiting satellite data. Remote Sens. Environ. 113 (8), 1700–1711.

Freeborn, P.H., Wooster, M.J., Roberts, G., 2011. Addressing the spatiotemporal sampling design of MODIS to provide estimates of the fire radiative energy emitted from Africa. Remote Sens. Environ. 115 (2), 475–489.

Freeborn, P.H., Wooster, M.J., Roy, D.P., Cochrane, M.A., 2014a. Quantification of MODIS fire radiative power (FRP) measurement uncertainty for use in satellite-based active fire characterization and biomass burning estimation. Geophys. Res. Lett. 41, 1988–1994.

Freeborn, P.H., Wooster, M.J., Roberts, G., Xu, W., 2014b. Evaluating the SEVIRI fire thermal anomaly detection algorithm across the Central African Republic using the MODIS active fire product. Remote Sens 6, 1890–1917.

Freeborn, P.H., Cochrane, M.A., Wooster, M.J., 2014c. A decade long, multi-scale map comparison of fire regime parameters derived from three publically available satellite-based fire products: a case study in the Central African Republic. Remote Sens. 6, 4061–4089.

Freeborn, P.H., Jolly, W.M., Cochrane, M.A., 2016. Impacts of changing fire weather conditions on reconstructed trends in US wildland fire activity from 1979 to 2014. J. Geophys. Res. Biogeosci. 121, 2856–2876.

Friedlingstein, P., O'sullivan, M., Jones, M.W., Andrew, R.M., Hauck, J., Olsen, A., Peters, G.P., Peters, W., Pongratz, J., Sitch, S., Le Quéré, C., 2020. Global carbon budget 2020. Earth Syst. Sci. Data 12, 3269–3340.

GCOS, 2016. The Global Observing System for Climate: Implementation Needs, GCOS-200. https://library.wmo.int/doc_num.php?explnum_id=3417 (last accessed March 2021).

Giglio, L., 2007. Characterization of the tropical diurnal fire cycle using VIRS and MODIS observations. Remote Sens. Environ. 407–421.

Giglio, L., Kendall, J.D., 2001. Application of the Dozier retrieval to wildfire characterization: a sensitivity analysis. Remote Sens. Environ. 77 (1), 34–49.

Giglio, L., Roy, D.P., 2020. On the outstanding need for a long-term, multi-decadal, validated and quality assessed record of global burned area: caution in the use of advanced very high resolution radiometer data. Sci. Remote Sens. 2, 100007.

Giglio, L., Schroeder, W., 2014. A global feasibility assessment of the bi-spectral fire temperature and area retrieval using MODIS data. Remote Sens. Environ. 152, 166–173.

Giglio, L., Kendall, J.D., Justice, C.O., 1999. Evaluation of global fire detection algorithms using simulated AVHRR infrared data. Int. J. Remote Sens. 20 (10), 1947–1985.

Giglio, L., Kendall, J.D., Tucker, C.J., 2000. Remote sensing of fires with the TRMM VIRS. Int. J. Remote Sens. 21 (1), 203–207.

Giglio, L., Descloitres, J., Justice, C.O., Kaufman, Y.J., 2003. An enhanced contextual fire detection algorithm for MODIS. Remote Sens. Environ. 87, 273–282.

Giglio, L., Csiszar, I., Justice, C., 2006. Global distribution and seasonality of active fires as observed with the terra and aqua moderate resolution imaging spectroradiometer (MODIS) sensors. J. Geophys. Res. Biogeosci. 111 https://doi.org/10.1029/2005JG000142. G2.

Giglio, L., Csiszar, I., Restás, Á., Morisette, J.T., Schroeder, W., Morton, D., Justice, C.O., 2008. Active fire detection and characterization with the advanced Spaceborne thermal emission and reflection radiometer (ASTER). Remote Sens. Environ. 112, 3055–3063.

Giglio, L., Randerson, J.T., van der Werf, G.R., 2013. Analysis of daily, monthly, and annual burned area using the fourth generation global fire emissions database (GFED4). J. Geophys. Res. Biogeosci. 118.

Giglio, L., Schroeder, W., Justice, C.O., 2016. The collection 6 MODIS active fire detection algorithm and fire products. Remote Sens. Environ. 178, 31–41.

Giglio, L., Boschetti, L., Roy, D.P., Humber, M.L., Justice, C.O., 2018. The collection 6 MODIS burned area mapping algorithm and product. Remote Sens. Environ. 217, 72–85.

Gill, A.M., 1975. Fire and the Australian flora: a review. Aust. For. 38, 4–25.

Gregoire, J.M., Simonetti, D., 2010. Interannual changes of fire activity in the protected areas of the SUN network and other parks and reserves of the west and Central Africa region derived from MODIS observations. Remote Sens. 2, 446–463.

Hall, J.V., Zhang, R., Schroeder, W., Huang, C., Giglio, L., 2019. Validation of GOES-16 ABI and MSG SEVIRI active fire products. Int. J. Appl. Earth Obs. Geoinf. 83, 101928.

Hally, B., Wallace, L., Reinke, K., Jones, S., 2017. A broad-area method for the diurnal characterisation of upwelling medium wave infrared radiation. Remote Sens. 9 (2), 167.

Hantson, S., Padilla, M., Corti, D., Chuvieco, E., 2013. Strengths and weaknesses of MODIS hotspots to characterize global fire occurrence. Remote Sens. Environ. 131, 152–159.

Henderson, S.B., Burkholder, B., Jackson, P.L., Brauer, M., Ichoku, C., 2008. Use of MODIS products to simplify and evaluate a forest fire plume dispersion model for PM10 exposure assessment. Atmos. Environ. 42, 8524–8532.

Hirsch, S.N., 1965. Airborne infrared mapping of forest fires. Fire. Technol 1 (4), 288–294.

Hirsch, K.G., 1991. A chronological overview of the 1989 fire season in Manitoba. For. Chron. 67 (4), 358–365.

Hirsch, E., Koren, I., 2021. Record-breaking aerosol levels explained by smoke injection into the stratosphere. Science 371 (6535), 1269–1274.

Huijnen, V., Wooster, M.J., Kaiser, J.W., Gaveau, D.L., Flemming, J., Parrington, M., Inness, A., Murdiyarso, D., Main, B., van Weele, M., 2016. Fire carbon emissions over maritime southeast Asia in 2015 largest since 1997. Sci. Rep. 6 (1), 1–8.

Hyer, E.J., Reid, J.S., Prins, E.M., Hoffman, J.P., Schmidt, C.C., Miettinen, J.I., Giglio, L., 2013. Patterns of fire activity over Indonesia and Malaysia from polar and geostationary satellite observations. Atmos. Res. 122, 504–519.

Ichoku, C., Ellison, L., 2014. Global top-down smoke aerosol emissions estimation using satellite fire radiative power measurements. Atmos. Chem. Phys. 14 (13), 6643–6667.

Ichoku, C., Kaufman, Y.J., 2005. A method to derive smoke emission rates from MODIS fire radiative energy measurements. IEEE Trans. Geosci. Rem. Sens. 43 (11), 2636–2649.

Ichoku, C., Remer, L.A., Kaufman, Y.J., Levy, R., Chu, D.A., Tanré, D., Holben, B.N., 2003. MODIS observation of aerosols and estimation of aerosol radiative forcing over southern Africa during SAFARI 2000. J. Geophys. Res.-Atmos. 108 (D13).

Ichoku, C., Giglio, L., Wooster, M.J., Remer, L.A., 2008. Global characterization of biomass-burning patterns using satellite measurements of fire radiative energy. Remote Sens. Environ. 112, 2950–2962.

Jaffe, D.A., O'Neill, S.M., Larkin, N.K., Holder, A.L., Peterson, D.L., Halofsky, J.E., Rappold, A.G., 2020. Wildfire and prescribed burning impacts on air quality in the United States. J. Air & Waste Manage. Assoc. 70 (6), 583–615.

Johnston, F.H., Henderson, S.B., Chen, Y., Randerson, J.T., Marlier, M., DeFries, R.S., Kinney, P., Bowman, D.M., Brauer, M., 2012. Estimated global mortality attributable to smoke from landscape fires. Environ. Health Perspect. 120 (5), 695–701.

Johnston, J.M., Wooster, M.J., Lynham, T.J., 2014. Experimental confirmation of the MWIR and LWIR grey body assumption for vegetation fire flame emissivity. Int. J. Wildland Fire 23 (4), 463–479.

Johnston, J.M., Jackson, N., McFayden, C., Ngo Phong, L., Lawrence, B., Davignon, D., Wooster, M.J., van Mierlo, H., Thompson, D.K., Cantin, A.S., Johnston, D., 2020. Development of the user requirements for the Canadian WildFireSat Satellite Mission. Sensors 20, 5081.

Johnston, J.M., Johnston, L.M., Wooster, M.J., Brookes, A., McFayden, C., Cantin, A.S., 2018a. Satellite detection limitations of sub-canopy smouldering wildfires in the North American Boreal Forest. Fire 1 (2), 28.

Johnston, J.M., Wheatley, M.J., Wooster, M.J., Paugam, R., Davies, G.M., DeBoer, K.A., 2018b. Flame-front rate of spread estimates for moderate scale experimental fires are strongly influenced by measurement approach. Fire 1 (1), 16.

Jordan, N.S., Ichoku, C., Hoff, R.M., 2008. Estimating smoke emissions over the US southern Great Plains using MODIS fire radiative power and aerosol observations. Atmos. Environ. 42 (9), 2007–2022.

Justice, C.O., Malingreau, J.P., Setzer, A.W., 1993. Satellite Remote Sensing of Fires- Potential and Limitations. Fire in the Environment- The Ecological, Atmospheric, and Climatic Importance of Vegetation Fires, 1993. John Wiley & Sons, Ltd, Chichester, United Kingdom, pp. 77–88.

Justice, C., Vermote, E., Townshend, J., Defries, R., Roy, D., Hall, D., Salomonson, V., Privette, J., Riggs, G., Strahler, A., Lucht, W., Myneni, R., Knyazikhin, Y., Running, S., Nemani, R., Wan, Z., Huete, A., van Leeuwen, W., Wolfe, R., Giglio, L., Muller, J.-P., Lewis, P., Barnsley, M., 1998. The Moderate Resolution Imaging Spectroradiometer (MODIS): land remote sensing for global change research. IEEE Trans. Geosci. Remote Sens. 36, 1228–1249.

Justice, C.O., Giglio, L., Korontzi, S., Owens, J., Morisette, J.T., Roy, D., Descloitres, J., Alleaume, S., Petitcolin, F., Kaufman, Y., 2002a. The MODIS fire products. Remote Sens. Environ. 83, 244–262.

Justice, C.O., Townshend, J.R.G., Vermote, E.F., Masuoka, E., Wolfe, R.E., Saleous, N., Roy, D.P., Morisette, J., 2002b. An overview of MODIS land data processing and product status. Remote Sens. Environ. 83, 3–15.

Kaiser, J.W., Heil, A., Andreae, M.O., Benedetti, A., Chubarova, N., Jones, L., Morcrette, J.J., Razinger, M., Schultz, M.G., Suttie, M., van der Werf, G.R., 2012. Biomass burning emissions estimated with a global fire assimilation system based on observed fire radiative power. Biogeosciences 9, 527–554.

Kaufman, Y.J., Tucker, C.J., Fung, I., 1990. Remote sensing of biomass burning in the tropics. J. Geophys. Res. 95, 9927–9939.

Kaufman, Y.J., Remer, L.A., Ottmar, R.D., Ward, D.E., Li, R.-R., Kleidman, R., Fraser, R. S., Flynn, L., McDougal, D., Shelton, G., 1996. Relationship between remotely sensed fire intensity and rate of emission of smoke: SCAR-C experiment. In: Levin, J. (Ed.), Global Biomass Burning. The MIT press, Cambridge, MA, pp. 685–696.

Kaufman, Y.J., Justice, C.O., Flynn, L.P., Kendall, J.D., Prins, E.M., Giglio, L., Ward, D.E., Menzel, W.P., Setzer, A.W., 1998. Potential global fire monitoring from EOS-MODIS. J. Geophys. Res.-Atmos. 103 (D24), 32215–32238.

Kaufman, Y.J., Tanré, D., Boucher, O., 2002. A satellite view of aerosols in the climate system. Nature 419 (6903), 215.

Kelley, D.I., Burton, C., Huntingford, C., Brown, M.A., Whitley, R., Dong, N., 2021. Low meteorological influence found in 2019 Amazonia fires. Biogeosciences 18 (3), 787–804.

Korontzi, S., McCarty, J., Loboda, T., Kumar, S., Justice, C., 2006. Global distribution of agricultural fires in croplands from 3 years of moderate resolution imaging spectroradiometer (MODIS) data. Glob. Biogeochem. Cycles 20 (2). https://doi.org/10.1029/2005GB002529.

Kremens, R.L., Dickinson, M.B., Bova, A.S., 2012. Radiant flux density, energy density, and fuel consumption in mixed-oak forest surface fires. Int. J. Wildland Fire 21, 722–730. https://doi.org/10.1071/WF10143.

Kumar, S.S., Roy, D.P., 2018. Global operational land imager (GOLI) Landsat-8 reflectance based active fire detection algorithm. Int. J. Digital Earth 11 (2), 154–178.

Laneve, G., Castronuovo, M.M., Cadau, E.G., 2006. Continuous monitoring of forest fires in the Mediterranean area using MSG. IEEE Trans. Geosci. Remote Sens. 44 (10), 2761–2768.

Langaas, S., 1992. Temporal and spatial distribution of savanna fires in Senegal and the Gambia, West Africa, 1989-90, derived from multi-temporal AVHRR night images. Int. J. Wildland Fire 2, 21–36.

Laris, P., 2002. Burning the seasonal mosaic: preventative burning strategies in the wooded savanna of southern Mali. Hum. Ecol. 30, 155–186.

Laurent, P., Mouillot, F., Moreno, M.V., Yue, C., Cias, P., 2019. Varying relationships between fire radiative power and fire size at a global scale. Biogeosciences 16, 275–288. https://doi.org/10.5194/bg-16-275-2019.

Le Page, Y., Oom, D., Silva, J.M.N., Jonsson, P., Pereira, J.M.C., 2010. Seasonality of vegetation fires as modified by human action: observing the deviation from eco-climatic fire regimes. Glob. Ecol. Biogeogr. 19, 575–588.

Lee, T.F., Tag, P.M., 1990. Improved detection of hotspots using the AVHRR 3.7 μm channel. Bull. Am. Meteorol. Soc. 71, 1722–1730.

Li, J., Roy, D.P., 2017. A global analysis of Sentinel-2A, Sentinel-2B and Landsat-8 data revisit intervals and implications for terrestrial monitoring. Remote Sens. 9 (9), 902.

Li, F., Zhang, X., Kondragunta, S., Roy, D.P., 2018. Investigation of the fire radiative energy biomass combustion coefficient: a comparison of polar and geostationary satellite retrievals over the conterminous United States. J. Geophys. Res. Biogeosci. https://doi.org/10.1002/2017JG004279.

Liu, T., Mickley, L.J., Marlier, M.E., DeFries, R.S., Khan, M.F., Latif, M.T., Karambelas, A., 2020. Diagnosing spatial biases and uncertainties in global fire emissions inventories: Indonesia as regional case study. Remote Sens. Environ. 237, 111557.

Lu, M., Li, F., Zhan, B., Li, H., Yang, X., Lu, X., Xiao, H., 2020. An improved cloud detection method for GF-4 imagery. Remote Sens. 12 (9), 1525.

Marchese, F., Mazzeo, G., Filizzola, C., Coviello, I., Falconieri, A., Lacava, T., Paciello, R., Pergola, N., Tramutoli, V., 2017. Issues and possible improvements in winter fires detection by satellite radiances analysis: lesson learned in two regions of northern Italy. IEEE J. Select. Top. Appl. Earth Observ. Remote Sens. 10 (7), 3297–3313.

Mathews, B.J., Strand, E.K., Smith, A.M., Hudak, A.T., Dickinson, B., Kremens, R.L., 2016. Laboratory experiments to estimate interception of infrared radiation by tree canopies. Int. J. Wildland Fire 25 (9), 1009–1014.

Matson, M., Dozier, J., 1981. Identification of subresolution high temperature sources using a thermal IR sensor. Photogramm. Eng. Remote. Sens. 47, 1311–1318.

Matson, M., Holben, B., 1986. Satellite detection of tropical burning in Brazil. Int. J. Remote Sens. 8 (3), 509–516. https://doi.org/10.1080/01431168708948657.

Matson, M., Stephens, G., Robinson, J., 1987. Fire detection using data from the NOAA-N satellites. Int. J. Remote Sens. 8 (7), 961–970.

McCarley, T.R., Hudak, A.T., Sparks, A.M., Vaillant, N.M., Meddens, A.J., Trader, L., Mauro, F., Kreitler, J., Boschetti, L., 2020. Estimating wildfire fuel consumption with multitemporal airborne laser scanning data and demonstrating linkage with MODIS-derived fire radiative energy. Remote Sens. Environ. 251, 112114.

McCarty, J.L., Korontzi, S., Justice, C.O., Loboda, T., 2009. The spatial and temporal distribution of crop residue burning in the contiguous United States. Sci. Total Environ. 407, 5701–5712.

McLauchlan, K.K., Higuera, P.E., Miesel, J., Rogers, B.M., Schweitzer, J., Shuman, J.K., Tepley, A.J., Varner, J.M., Veblen, T.T., Adalsteinsson, S.A., Balch, J.K., 2020. Fire as a fundamental ecological process: research advances and frontiers. J. Ecol. 108, 2047–2069.

Morisette, J.T., Giglio, L., Csiszar, I., Justice, C.O., 2005. Validation of the MODIS active fire product over Southern Africa with ASTER data. Int. J. Remote Sens. 26 (19), 4239–4264.

Mota, B., Wooster, M.J., 2018. A new top-down approach for directly estimating biomass burning emissions and fuel consumption rates and totals from geostationary satellite fire radiative power (FRP). Remote Sens. Environ. 206, 45–62.

Mouillot, F., Schultz, M.G., Yue, C., Cadule, P., Tansey, K., Ciais, P., Chuvieco, E., 2014. Ten years of global burned area products from spaceborne remote sensing—a review: analysis of user needs and recommendations for future developments. Int. J. Appl. Earth Obs. Geoinf. 26, 64–79.

Muirhead, K., Cracknell, A.P., 1985. Straw burning over Great Britain detected by AVHRR. Int. J. Remote Sens. 6, 827–833. https://doi.org/10.1080/01431168508948506.

Nguyen, H.M., Wooster, M.J., 2020. Advances in the estimation of high Spatio-temporal resolution pan-African top-down biomass burning emissions made using geostationary fire radiative power (FRP) and MAIAC aerosol optical depth (AOD) data. Remote Sens. Environ. 248, 111971.

Parent, G., Acem, Z., Lechêne, S., Boulet, P., 2010. Measurement of infrared radiation emitted by the flame of a vegetation fire. Int. J. Therm. Sci. 49 (3), 555–562.

Pastor, E., Àgueda, A., Andrade-Cetto, J., Muñoz, M., Pérez, Y., Planas, E., 2006. Computing the rate of spread of linear flame fronts by thermal image processing. Fire Saf. J. 41 (8), 569–579.

Paugam, R., Wooster, M.J., Roberts, G., 2012. Use of handheld thermal imager data for airborne mapping of fire radiative power and energy and flame front rate of spread. IEEE Trans. Geosci. Remote Sens. 51 (6), 3385–3399.

Pereira, M.C., Setzer, A.W., 1993. Spectral characteristics of fire scars in Landsat-5 TM images of Amazonia. Int. J. Remote Sens. 14, 2061–2078.

Pricope, N.G., Binford, M.W., 2012. A spatio-temporal analysis of fire recurrence and extent for semi-arid savanna ecosystems in southern Africa using moderate-resolution satellite imagery. J. Environ. Manag. 100, 72–85.

Prins, E.M., Menzel, W.P., 1992. Geostationary satellite detection of biomass burning in South America. Int. J. Remote Sens. 13 (15), 2783–2799.

Prins, E.M., Menzel, W.P., 1994. Trends in South American biomass burning detected with the GOES visible infrared spin scan radiometer atmospheric sounder from 1983 to 1991. J. Geophys. Res.-Atmos. 99 (D8), 16719–16735.

Prins, E., Feltz, J., Menzel, W., Ward, D., 1998. An overview of GOES-8 diurnal fire and smoke results for SCAR-B and 1995 fire season in South America. J. Geophys. Res.-Atmos. 31821–31835.

Realmuto, V.J., Dennison, P.E., Foote, M., Ramsey, M.S., Wooster, M.J., Wright, R., 2015. Specifying the saturation temperature for the HyspIRI 4-μm channel. Remote Sens. Environ. 167, 40–52.

Reid, J.S., Hyer, E.J., Prins, E.M., Westphal, D.L., Zhang, J., Wang, J., Christopher, S.A., Curtis, C.A., Schmidt, C.C., Eleuterio, D.P., Richardson, K.A., 2009. Global monitoring and forecasting of biomass-burning smoke: description of and lessons from the fire locating and modeling of burning emissions (FLAMBE) program. IEEE J. Select. Top. Appl. Earth Observ. Remote Sens. 2 (3), 144–162.

Riggan, P.J., Tissell, R.G., Lockwood, R.N., Brass, J.A., Pereira, J.A.R., Miranda, H.S., Miranda, A.C., Campos, T., Higgins, R., 2004. Remote measurement of energy and carbon flux from wildfires in Brazil. Ecol. Appl. 14 (3), 855–872.

Roberts, G., Wooster, M.J., 2008. Fire detection and fire characterization over africa using meteosat SEVIRI. IEEE Trans. Geosci. Remote Sens. 48 (4), 1200–1219.

Roberts, G., Wooster, M.J., 2014. Development of a multi-temporal Kalman filter approach to geostationary active fire detection & fire radiative power (FRP) estimation. Remote Sens. Environ. 152, 392–412.

Roberts, G., Wooster, M.J., 2021. Global impact of landscape fire emissions on surface level PM2. 5 concentrations, air quality exposure and population mortality. Atmos. Environ. 118210.

Roberts, G., Wooster, M.J., Perry, G.L., Drake, N., Rebelo, L.M., Dipotso, F., 2005. Retrieval of biomass combustion rates and totals from fire radiative power observations: application to southern Africa using geostationary SEVIRI imagery. J. Geophys. Res.-Atmos. 110. D21.

Roberts, G., Wooster, M., Lagoudakis, E., 2009. Annual and diurnal African biomass burning temporal dynamics. Biogeosciences 849–866.

Roberts, G., Wooster, M., Freeborn, P.H., Xu, W., 2011. Integration of geostationary FRP and polar-orbiter burned area datasets for an enhanced biomass burning inventory. Remote Sens. Environ. 115, 2047–2061.

Roberts, G., Wooster, M.J., Xu, W., Freeborn, P.H., Morcrette, J.-J., Jones, L., Benedetti, A., Kaiser, J., 2015. LSA SAF Meteosat FRP Products : part 2 – Evaluation and demonstration of use in the Copernicus Atmosphere Monitoring Service (CAMS). Atmos. Chem. Phys. 15, 13241–13267.

Roberts, G., Wooster, M.J., Xu, W., He, J., 2018a. Fire activity and fuel consumption dynamics in sub-Saharan Africa. Remote Sens. 10 (10), 1591.

Roberts, G., Wooster, M.J., Lauret, N., Gastellu-Etchegorry, J.P., Lynham, T., McRae, D., 2018b. Investigating the impact of overlying vegetation canopy structures on fire radiative power (FRP) retrieval through simulation and measurement. Remote Sens. Environ. 217, 158–171.

Rogers, B.M., Balch, J.K., Goetz, S.J., Lehmann, C.E., Turetsky, M., 2020. Focus on changing fire regimes: interactions with climate, ecosystems, and society. Environ. Res. Lett. 15, 30201.

Ross, A.N., Wooster, M.J., Boesch, H., Parker, R., 2013. First satellite measurements of carbon dioxide and methane emission ratios in wildfire plumes. Geophys. Res. Lett. 40 (15), 4098–4102.

Roteta, E., Bastarrika, A., Padilla, M., Storm, T., Chuvieco, E., 2019. Development of a Sentinel-2 burned area algorithm: generation of a small fire database for sub-Saharan Africa. Remote Sens. Environ. 222, 1–17.

Roy, D.P., Boschetti, L., Justice, C.O., Ju, J., 2008. The collection 5 MODIS burned area product - global evaluation by comparison with the MODIS active fire product. Remote Sens. Environ. 112, 3690–3707.

Roy, D.P., Huang, H., Boschetti, L., Giglio, L., Yan, L., Zhang, H.K., Li, Z., 2019. Landsat-8 and Sentinel-2 burned area mapping - a combined sensor multi-temporal change detection approach. Remote Sens. Environ. 231, 111254.

Schmit, T.J., Griffith, P., Gunshor, M.M., Daniels, J.M., Goodman, S.J., Lebair, W.J., 2017. A closer look at the ABI on the GOES-R series. Bull. Am. Meteorol. Soc. 98 (4), 681–698.

Scholes, R.J., Kendall, J., Justice, C.O., 1996. The quantity of biomass burned in southern Africa. J. Geophys. Res.-Atmos. 101 (D19), 23667–23676.

Schroeder, W., Prins, E., Giglio, L., Csiszar, I., Schmidt, C., Morisette, J., Morton, D., 2008. Validation of GOES and MODIS active fire detection products using ASTER and ETM+ data. Remote Sens. Environ. 112 (5), 2711–2726.

Schroeder, W., Oliva, P., Giglio, L., Csiszar, I., 2014. The new VIIRS 375 m active fire detection data product: algorithm description and initial assessment. Remote Sens. Environ. 143, 85–96.

Schroeder, W., Oliva, P., Giglio, L., Quayle, B., Lorenz, E., Morelli, F., 2016. Active fire detection using Landsat-8/OLI data. Remote Sens. Environ. 185, 210–220.

Seiler, W., Crutzen, P.J., 1980. Estimates of gross and net fluxes of carbon between the biosphere and the atmosphere from biomass burning. Climate Change 2, 207–248.

Sembhi, H., Wooster, M., Zhang, T., Sharma, S., Singh, N., Agarwal, S., Boesch, H., Gupta, S., Misra, A., Tripathi, S.N., Mor, S., 2020. Post-monsoon air quality degradation across Northern India: assessing the impact of policy-related shifts in timing and amount of crop residue burnt. Environ. Res. Lett. 15, 104067.

Setzer, A.W., Pereira, M.C., 1991. Amazonia biomass burnings n 1987 and an estimated of their tropospheric emissions. Ambio 20 (1), 19–22.

Shephard, M.W., Kennelly, E.J., 2003. Effect of band-to-band coregistration on fire property retrievals. IEEE Trans. Geosci. Remote Sens. 41 (11), 2648–2661.

Smith, A.M.S., Wooster, M.J., 2005. Remote classification of head and backfire types from MODIS fire radiative power and smoke plume observations. Int. J. Wildland Fire 14, 249–254.

Smith, A.M.S., Tinkham, W.T., Roy, D.P., Boschetti, L., Kremens, R.L., Kumar, S.S., Sparks, A.M., Falkowski, M.J., 2013. Quantification of fuel moisture effects on biomass consumed derived from fire radiative energy retrievals. Geophys. Res. Lett. 40 (23), 6298–6302. https://doi.org/10.1002/2013GL058232.

Smith, A.M.S., Sparks, A.M., Kolden, C.A., Abatzoglou, J.T., Talhelm, A.F., Johnson, D. M., Boschetti, L., Lutz, J.A., Apostol, K.G., Yedinak, K.M., Tinkham, W.T., Kremens, R.J., 2016. Towards a new paradigm in fire severity research using dose-response experiments. Int. J. Wildland Fire 25, 158–166.

Smith, A.M.S., Talhelm, A.F., Johnson, D.M., Sparks, A.M., Yedinak, K.M., Apostol, K.G., Tinkham, W.T., Kolden, C.A., Abatzoglou, J.T., Lutz, J.A., Davis, A.S., Pregitzer, K.S., Adams, H.D., Kremens, R.L., 2017. Effects of fire radiative energy density doses on Pinus contorta and Larix occidentalis seedling physiology and mortality. Int. J. Wildland Fire 26 (1), 82–94.

Sofiev, M., Vankevich, R., Lotjonen, M., Prank, M., Petukhov, V., Ermakova, T., Koskinen, J., Kukkonen, J., 2009. An operational system for the assimilation of the satellite information on wild-land fires for the needs of air quality modelling and forecasting. Atmos. Chem. Phys. 9, 6833–6847. https://doi.org/10.5194/acp-9-6833-2009.

Soja, A.J., Sukhinin, A.I., Cahoon, D.R., Shugart, H.H., Stackhouse, P.W., 2004. AVHRR-derived fire frequency, distribution and area burned in Siberia. Int. J. Remote Sens. 25, 1939–1960.

Sommers, W.T., Loehman, R.A., Hardy, C.C., 2014. Wildland fire emissions, carbon, and climate: science overview and knowledge needs. For. Ecol. Manag. 317, 1–8.

Sparks, A.M., Smith, A.M., Talhelm, A.F., Kolden, C.A., Yedinak, K.M., Johnson, D.M., 2017. Impacts of fire radiative flux on mature Pinus ponderosa growth and vulnerability to secondary mortality agents. Int. J. Wildland Fire 26 (1), 95–106.

Sparks, A.M., Kolden, C.A., Smith, A.M., Boschetti, L., Johnson, D.M., Cochrane, M.A., 2018. Fire intensity impacts on post-fire temperate coniferous forest net primary productivity. Biogeosciences 15 (4), 1173.

Stott, P., 2000. Combustion in tropical biomass fires: a critical review. Prog. Phys. Geogr. 24 (3), 355–377.

Stroppiana, D., Pinnock, S., Gregoire, J.M., 2000. The global fire product: daily fire occurrence from April 1992 to December 1993 derived from NOAA AVHRR data. Int. J. Remote Sens. 21 (6–7), 1279–1288.

Sullivan, A.L., Ellis, P.F., Knight, I.K., 2003. A review of radiant heat flux models used in bushfire applications. Int. J. Wildland Fire 12 (1), 101–110.

Trigg, S.N., Roy, D.P., 2007. A focus group study of factors that promote and constrain the use of satellite derived fire products by resource managers in southern Africa. J. Environ. Manag. 82, 95–110.

Udahemuka, G., van den Bergh, F., van Wyk, B.J., van Wyk, M.A., 2007. Robust fitting of the diurnal brightness temperature cycle. In: 18th Annual Symposium of the Pattern Recognition Association of South Africa (PRASA), p. 6. Pietermaritzburg, Kwazulu-Natal, South Africa. 28-30 November 2007.

van den Bergh, F., Frost, P.E., 2005. A multitemporal approach to fire detection using MSG data. In: Proceedings 2nd IEEE International Workshop Analysis Multi-Temporal Remote Sensing Images. May 16–18, 2005, pp. 156–160.

van den Bergh, F., Udahemuka, G., van Wyk, B.J., 2009. Potential fire detection based on Kalman-driven change detection. In: International Geoscience and Remote Sensing Symposium. IGARSS 2009. 12-17 July, pp. 77–80.

Van der Werf, G.R., Randerson, J.T., Giglio, L., Collatz, G.J., Mu, M., Kasibhatla, P.S., Morton, D.C., DeFries, R.S., Jin, Y.V., van Leeuwen, T.T., 2010. Global fire emissions and the contribution of deforestation, savanna, forest, agricultural, and peat fires (1997–2009). Atmos. Chem. Phys. 10 (23), 11707–11735.

van der Werf, G.R., Randerson, J.T., Giglio, L., Van Leeuwen, T.T., Chen, Y., Rogers, B. M., Mu, M., Van Marle, M.J., Morton, D.C., Collatz, G.J., Yokelson, R.J., 2017. Global fire emissions estimates during 1997–2016. Earth Syst. Sci. Data 9 (2), 697.

Veraverbeke, S., Hook, S.J., 2013. Evaluating spectral indices and spectral mixture analysis for assessing fire severity, combustion completeness and carbon emissions. Int. J. Wildland Fire 22 (5), 707–720.

Vermote, E., Ellicott, E., Dubovik, O., Lapyonok, T., Chin, M., Giglio, L., Roberts, G.J., 2009. An approach to estimate global biomass burning emissions of organic and black carbon from MODIS fire radiative power. J. Geophys. Res.-Atmos. 114 (D18).

Weaver, J.F., Purdom, J.F., Schneider, T.L., 1995. Observing forest fires with the GOES-8, 3.9-μm imaging channel. Weather Forecast. 10, 4.803–808.

Whitlock, C., Higuera, P.E., McWethy, D.B., Briles, C.E., 2010. Paleoecological perspectives on fire ecology: revisiting the fire-regime concept. Open Ecol. J. 3 (1), 6–23.

Wickramasinghe, C.H., Jones, S., Reinke, K., Wallace, L., 2016. Development of a multi-spatial resolution approach to the surveillance of active fire lines using Himawari-8. Remote Sens. 8 (11), 932.

Wiedinmyer, C., Akagi, S.K., Yokelson, R.J., Emmons, L.K., Al-Saadi, J.A., Orlando, J.J., Soja, A.J., 2011. The Fire INventory from NCAR (FINN): a high resolution global model to estimate the emissions from open burning. Geosci. Model Dev. 4 (3), 625.

Wooster, M.J., Rothery, D.A., 1997. Time-series analysis of effusive volcanic activity using the ERS along track scanning radiometer: the 1995 eruption of Fernandina volcano, Galápagos Islands. Remote Sens. Environ. 62 (1), 109–117.

Wooster, M.J., Zhang, Y.H., 2004. Boreal forest fires burn less intensely in Russia than in North America. Geophys. Res. Lett. 31.

Wooster, M.J., Zhukov, B., Oertel, D., 2003. Fire radiative energy for quantitative study of biomass burning: derivation from the BIRD experimental satellite and comparison to MODIS fire products. Remote Sens. Environ. 86, 83–107.

Wooster, M.J., Perry, G.L.W., Zhukov, B., Oertel, D., 2004. Estimation of energy emissions, fireline intensity and biomass consumption in wildland fires: a potential approach using remotely sensed fire radiative energy. In: Spatial Modeling of the Terrestrial Environment. John Wiley & Sons, pp. 175–196.

Wooster, M.J., Roberts, G., Perry, G.L.W., Kaufman, Y.J., 2005. Retrieval of biomass combustion rates and totals from fire radiative power observations: FRP derivation and calibration relationships between biomass consumption and fire radiative energy release. J. Geophys. Res. 110, D24311 https://doi.org/10.1029/2005JD006318.

Wooster, M.J., Perry, G.L.W., Zoumas, A., 2012a. Fire, drought and El Nino relationships on Borneo (Southeast Asia) in the pre-MODIS era (1980-2000). Biogeosciences 9, 317–340.

Wooster, M.J., Xu, W., Nightingale, T., 2012b. Sentinel-3 SLSTR active fire detection and FRP product: Pre-launch algorithm development and performance evaluation using MODIS and ASTER datasets. Remote Sens. Environ. 120, 236–254.

Wooster, M.J., Roberts, G., Freeborn, P.H., Xu, W., Govaerts, Y., Beeby, R., He, J., Lattanzio, A., Mullen, R., 2015. Meteosat SEVIRI Fire Radiative Power (FRP) products from the Land Surface Analysis Satellite Applications Facility (LSA SAF) – Part 1 : algorithms, product contents and analysis. Atmos. Chem. Phys. 15, 9815–9895.

Wooster, M.J., Gaveau, D., Salim, M.A., Zhang, T., Xu, W., Green, D.C., Huijnen, V., Murdiyarso, D., Gunawan, D., Borchard, N., Schirrmann, M., 2018. New tropical peatland gas and particulate emissions factors indicate 2015 Indonesian fires released far more particulate matter (but less methane) than current inventories imply. Remote Sens. 10 (4), 495.

Xu, W., Wooster, M.J., Roberts, G., Freeborn, P., 2010. New GOES imager algorithms for cloud and active fire detection and fire radiative power assessment across North, South and Central America. Remote Sens. Environ. 114, 1876–1895.

Xu, W., Wooster, M.J., Kaneko, T., He, J.P., Zhang, T.R., Fisher, D., 2017. Major advances in geostationary fire radiative power (FRP) retrieval over Asia and Australia stemming from use of Himarawi-8 AHI. Remote Sens. Environ. 193, 138–149.

Xu, W., Wooster, M.J., He, J., Zhang, T., 2020. First study of Sentinel-3 SLSTR active fire detection and FRP retrieval: night-time algorithm enhancements and global intercomparison to MODIS and VIIRS AF products. Remote Sens. Environ. 248, 111947.

Xu, W., Wooster, M.J., He, J., Zhang, T., 2021a. Improvements in high-temporal resolution active fire detection and FRP retrieval over the Americas using GOES-16 ABI with the geostationary fire thermal anomaly (FTA) algorithm. Sci. Remote Sens. 3, 100016.

Xu, W., Wooster, M.J., Polehampton, E., Yemelyanova, R., Zhang, T., 2021b. Sentinel-3 active fire detection and FRP product performance-Impact of scan angle and SLSTR middle infrared channel selection. Remote Sens. Environ. 261, 112460.

Yang, J., Zhang, Z., Wei, C., Lu, F., Guo, Q., 2017. Introducing the new generation of Chinese geostationary weather satellites, Fengyun-4. Bull. Am. Meteorol. Soc. 98 (8), 1637–1658.

Yin, L., Du, P., Zhang, M., Liu, M., Xu, T., Song, Y., 2019. Estimation of emissions from biomass burning in China (2003–2017) based on MODIS fire radiative energy data. Biogeosciences 16 (7), 1629–1640.

Zhang, X.S., Kondragunta, S., Ram, J., Schmidt, C., Huang, H.C., 2012. Near-real-time global biomass burning emissions product from geostationary satellite constellation. J. Geophys. Res.-Atmos. 117 (D14) https://doi.org/10.1029/2012JD017459.

Zhang, X.S., Kondragunta, S., Roy, D.P., 2014a. Interannual variation in biomass burning and fire seasonality derived from geostationary satellite data across the contiguous United States from 1995 to 2011. J. Geophys. Res. Biogeosci. 119, 1147–1162.

Zhang, F., Wang, J., Ichoku, C., Hyer, E., Yang, Z., Ge, C., Su, S., Zhang, X., Kondragunta, S., Kaiser, J., Wiedinmyer, C., da Silva, A., 2014b. Sensitivity of mesoscale modeling of smoke direct radiative effect to the emission inventory: a case study in northern sub-Saharan African region. Environ. Res. Lett. 9, 075002.

Zhang, T., Wooster, M.J., Xu, W., 2017. Approaches for synergistically exploiting VIIRS I- and M-Band data in regional active fire detection and FRP assessment: a demonstration with respect to agricultural residue burning in Eastern China. Remote Sens. Environ. 198, 407–424.

Zhang, T., Wooster, M.J., de Jong, M.C., Xu, W., 2018. How well does the 'small fire boost' methodology used within the GFED4. 1s fire emissions database represent the timing, location and magnitude of agricultural burning? Remote Sens. 10 (6), 823.

Zhang, T., de Jong, M.C., Wooster, M.J., Xu, W., Wang, L., 2020. Trends in eastern China agricultural fire emissions derived from a combination of geostationary (Himawari) and polar (VIIRS) orbiter fire radiative power products. Atmos. Chem. Phys. 20 (17), 10687–10705.

Zhukov, B., Lorenz, E., Oertel, D., Wooster, M., Roberts, G., 2006. Spaceborne detection and characterization of fires during the bi-spectral infrared detection (BIRD) experimental small satellite mission (2001–2004). Remote Sens. Environ. 100 (1), 29–51.